CERN-TH. 95-283

SPACE, TIME AND COLOR IN HADRON PRODUCTION VIA $e^+e^- \to Z^0$ AND $e^+e^- \to W^+W^-$

John Ellis and Klaus Geiger

CERN TH-Division, CH-1211 Geneva 23, Switzerland

Abstract

The time-evolution of jets in hadronic e^+e^- events at LEP is investigated in both position- and momentum-space, with emphasis on effects due to color flow and particle correlations. We address dynamical aspects of the four simultanously-evolving, cross-talking parton cascades that appear in the reaction $e^+e^- \to \gamma^*/Z^0 \to W^+W^- \to q_1\bar{q}_2q_3\bar{q}_4$, and compare with the familiar two-parton cascades in $e^+e^- \to Z^0 \to q_1\bar{q}_2$. We use a QCD statistical transport approach, in which the multiparticle final state is treated as an evolving mixture of partons and hadrons, whose proportions are controlled by their local space-time geography via standard perturbative QCD parton shower evolution and a phenomenological model for non-perturbative parton-cluster formation followed by cluster decays into hadrons. Our numerical simulations exhibit a characteristic 'inside-outside' evolution simultanously in position and momentum space. We compare three different model treatments of color flow, and find large effects due to cluster formation by the combination of partons from different W parents. In particular, we find in our preferred model a shift of several hundred MeV in the apparent mass of the W, which is considerably larger than in previous model calculations. This suggests that the determination of the W mass at LEP2 may turn out to be a sensitive probe of spatial correlations and hadronization dynamics.

johne@cernvm.cern.ch

klaus@surya11.cern.ch

CERN-TH. 95-283, October 1995

1. INTRODUCTION

One of the primary physics topics at the second phase of the CERN e^+e^- collider LEP is expected to be the determination of the $W^\pm$ mass. Because of the higher statistics and the possibility of using more kinematic constraints in the absence of energetic neutrinos from leptonic $W^\pm$ decays, there is great interest in using purely hadronic decays of W^+W^- pairs. A major challenge in the analysis of these events is the assignment of the observed hadrons to the parent $W^\pm$, which may alternatively be regarded as a novel opportunity to study 'non-trivial' space, time and color correlations of multiple partons in the production and decay of W^+W^- pairs. Compared with jet fragmentation in e^+e^- collisions on the Z^0 peak, the expected new physics aspects are due to the fact that the W^+ and W^- decay very rapidly after their production into two jets each, while they are still practically on top of one other. Hence, one must deal with an initial parton configuration consisting of two quark-antiquark pairs that are produced very close in both space and time. The subsequent evolution of the system via parton showering and parton-hadron conversion is therefore subject to interference and combination between the decay products of the $W^\pm$, and correlation effects due to the local density of particles. This situation is to be contrasted with the more familiar two-jet events, in which a single back-to-back initial pair of partons evolves essentially unscathed in empty space.

Treating these interference, combination and correlation effects certainly requires a detailed understanding of color structure in the development of hadronic showers. This has become available during the past few years, as analytical perturbative QCD calculations within the modified leading-logarithmic approximation [1] have matured to provide a quantitative description of color flow phenomena in jet events. Moreover, the effect of the calculated perturbative color structure on the non-perturbative hadronization process has been considered within the local parton-hadron duality framework [2]. The results have included detailed predictions for many hadronic observables, which have been found to agree remarkably well with experimental data from LEP1 experiments on the Z^0 peak [3].

The prospective scenario of cross-talking jets and the resulting complications associated with multi-particle evolution has, moreover, recently attracted considerable attention to color correlation and interference effects associated with the randomization and statistical rearrangement of the color flow in W^+W^- events at LEP2. Perturbative aspects of this

physics have been studied in a number of papers by the Durham-St. Petersburg group [4, 5, 6], and phenomenological non-perturbative aspects have been investigated by various authors in Refs. [7, 8, 9, 10, 11, 12, 13]. In particular, Sjöstrand and Khoze [8] have discussed in great detail interference and color reconnection effects in overlapping jet configurations during both the perturbative QCD regime of parton evolution, where they are suppressed by $O(\alpha_s^2/N_c^2)$, and the non-perturbative conversion of partons into final-state hadrons. The perturbative analysis is firmly based on the fundamentals of QCD, but in our present state of ignorance the non-perturbative aspects require a phenomenological description of the hadronization process. In Ref. [8] this was addressed within the Lund string-fragmentation model [14], whereas in Ref. [10] the Marchesini-Webber model [15] was employed. A common feature of both approaches was the use of a particular model for the rearrangement of color in hadronization, which is modelled as a "color reconnection" of final-state partons, in which some *ad hoc* elements are required (see Ref. [10] for an overview of such color reconnection models).

These previous works have reached the important conclusions that, on the one hand, perturbative color rearrangement and interference effects are negligibly small, but, on the other hand, final-state interactions in the process of hadron formation may lead to a significant systematic shift in the mass of the $W^{\pm}$ which could have far-reaching implications for its determination at LEP2. Since parton-hadron transmutation is currently not calculable from first principles, but requires model assumptions, the latter conclusion is necessarily model-dependent, and a comparison of different approaches is therefore desirable.

We think it may be useful to complement previous approaches by considering the full space-time history of the dynamically-evolving particle system, so that the correlations of partons in space and time can be taken fully into account when hadronization is modelled. With this motivation in mind, we develop two new features in the present work:

(i) we provide and test an alternative description of the interplay between parton evolution and hadronization, in which we trace the microscopic history of the particle dynamics in both space-time and momentum space, and

(ii) we study the possible observable effects of multi-parton correlations in hadronic e^+e^--events using a different space-time model of the parton-hadron conversion process.

These features enable us to compare the dynamics of ordinary 2-jet events with the evolution of 4-jet events that consist of two overlapping and simultanously-evolving 2-jets in a way that differs from previous approaches, and thus may cast useful light on the possible model-dependence of their results.

The central element in our approach is the use of QCD transport theory [16] and quantum field kinetics [17] to follow the evolution of the multi-jet system in 7-dimensional phase-space $d^3rd^3kdk^0$. We include both the perturbative QCD parton-shower development [1, 18, 19], and the phenomenological parton-hadron conversion model which we proposed recently [20], considering dynamical parton-cluster formation as primarily dependent on spatial separation, which is followed by the decay of clusters into hadrons. This approach may be extended to situations involving more complicated initial states, as in e-p, p-p, e-nucleus, p-nucleus and nucleus-nucleus collisions. However, the fact that the initial state is unambiguous in e^+e^- collisions provides a particularly clean laboratory for studying the differences between our approach and others, which is also of great topical relevance. Specifically, in this paper we compare

$$e^+e^- \ \rightarrow \ Z^0 \ \rightarrow \ q_1\bar{q}_2 \ \rightarrow \ hadrons \tag{1}$$

at a center-of-mass energy of 91 GeV as at LEP1 with

$$e^+e^- \ \rightarrow \ \gamma^*/Z^0 \ \rightarrow \ W^+W^- \ \rightarrow \ q_1\bar{q}_2q_3\bar{q}_4 \ \rightarrow \ hadrons \tag{2}$$

at a center-of-mass energy of 170 GeV as at LEP2. The theoretical description of both the parton-shower evolution and the hadronization of the produced quarks and gluons should be of the same generic pattern in these two cases, namely time-like parton cascades with hadron formation in vacuum, i.e., in the absence of beam remnants or surrounding matter. This enables key aspects of our approach to be isolated and compared with previous approaches. Since QCD at LEP1 is nowadays very well understood and described impressively accurately [21] by various Monte Carlo models [22, 23, 24], the reaction (1) provides a testing ground for our distinct approach, as well as a baseline for extracting new physics aspects in the reaction (2) at LEP2.

This paper is organized as follows. In Sec. 2 we review our transport-theoretical approach to the space-time description of general high-energy QCD processes, and describe different ways of incorporating color degrees of freedom, a feature we had not addressed

previously. To assess the model-dependence of the effects of color flow on the space-time evolution, we define 3 distinct scenarios. One does not consider color at all, as in our previous work, in a second scenario the color flow is traced so that only color-singlet configurations of two partons participate in hadronization, and in the third variant arbitrary color configurations participate in hadronization, with hadrons emerging from color-singlet components and the initial net color being locally balanced by parton emission. Sec. 3 is then devoted to the application and systematic analysis of this formalism to hadronic e^+e^- events of the types (1) and (2). We demonstrate the emergence of the inside-out cascade picture [25, 26] in these reactions, and compare the above three scenarios for taking account of color degrees of freedom, confronting characteristic event properties and observables in the three cases. We target special attention on the W mass determination in 4-jet events (2), simulating the experimental reconstruction of jets and exploring how the apparent W mass may be shifted by the previous space-time history of the system, in particular by interference between the parton showers produced in the decays of the two different W particles. Finally, in Sec. 4 we discuss the interpretation of our results, which suggest that the W mass shift may be even larger than that found in previous studies [8, 10]. Much of this substantial difference in the magnitude of particle- and color-correlation effects from the previous investigations of Refs. [8, 10] may be due to the fact that our hadronization Ansatz allows partons to form clusters 'exogamously' without any regard to their origins in the two perturbative W showers, the sole criterion being their spatial separations. This aspect is significant in the particular space-time geography of W^+W^- events (2), in which the wee partons from the two parton showers overlap strongly in the neighborhood of the W^+W^- production vertex.

2. KINETIC APPROACH TO PARTON EVOLUTION AND HADRONIZATION

In the first part of this section, we review essential elements of the kinetic approach [20] to the dynamical description of perturbative QCD shower development and parton-hadron conversion that we introduced previously, which incorporates spatial information in an essential way. Then we provide a first discussion of color flow within this framework, proposing three scenarios for the treatment of color degrees of freedom in cluster formation.

In the last part of this Section, we outline the practical calculation scheme that we use in Section 3 as the basis for a Monte Carlo simulation of the space-time development of e^+e^--collisions.

2.1 Review of our Model

In a previous paper [20] we presented in detail our approach to the problem of hadronization of quarks and gluons in conjunction with the space-time evolution of parton showers produced by hard QCD processes in high-energy reactions, such as e^+e^- collisions, deep-inelastic ep scattering, hadron-hadron and eventually nucleus-nucleus collisions. Here we just sketch the main features of our model, and refer the interested reader to our previous paper for more details.

In order to model the dynamical transition between the perturbative and non-perturbative domains of QCD, we advocate a combination of perturbative QCD and effective field theory in their respective domains of validity, and describe the conversion between them using ideas developed in phenomenological descriptions of the finite-temperature transition from a quark-gluon plasma to a hadronic phase [27]. The latter is described by an effective theory incorporating a chiral field U whose vacuum expectation value (vev) $U_0 \equiv \langle 0|U + U^\dagger|0\rangle$ represents the non-perturbative quark condensate $\langle 0|\bar{q}q|0\rangle$, and a scalar field χ whose vev $\chi_0 \equiv \langle 0|\chi|0\rangle$ represents the non-perturbative gluon condensate $\langle 0|F_{\mu\nu}F^{\mu\nu}|0\rangle$. We visualize hard scattering in high-energy processes as producing a "hot spot", in which the usual long-range order represented by U_0 and χ_0 is disrupted locally by the appearance of a bubble of the naive perturbative vacuum in which $\langle 0|\bar{q}q|0\rangle = 0 = \langle 0|F_{\mu\nu}F^{\mu\nu}|0\rangle$. Within this bubble, a parton shower develops in the usual perturbative way, with the hot spot expanding and cooling in an irregular stochastic manner described by QCD transport equations [17]. This perturbative description remains appropriate in any phase-space region of the shower where the local energy density is large compared to the difference in energy density between the perturbative partonic and the non-perturbative hadronic vacua. When this condition is no longer satisfied, a hadronic bubble [1] may be formed with a probability determined by statistical-mechanical considerations. A complete description of this conversion requires a

[1] Specifically, this bubble has quantum numbers matching those of the parent partons, and contains both gluonic (χ) and chiral (U) degrees of freedom. We acknowledge critical questions from T. Sjöstrand on this point.

treatment combining partonic and hadronic degress of freedom, which is an essential aspect of our approach.

2.1.1 Scale-Dependent Effective Lagrangian

The theoretical basis for the above intuitive picture is provided by a gauge-invariant effective Lagrangian that embodies both fundamental partonic degrees and effective hadronic degrees of freedom. It depends explicitly on the space-time scale L (specified below) which characterizes locally the relevant dynamical processes of the physical system under consideration. As we shall see later, the appropriate space-time scale L in any region of a hadronic shower is governed locally by the dynamical evolution of the system itself, through kinetic equations that are constrained by the uncertainty principle, and incorporate both space-time and energy-momentum variables. Our Lorentz-invariant measure L of the space-time separation between two color charges located at r_i and r_j where $r \equiv r^\mu = (t, \vec{r})$ is defined by

$$L(r_i, r_j) \; := \; \sqrt{(r_i - r_j)_\mu (r_i - r_j)^\mu} \; , \tag{3}$$

We introduce phenomenologically a confinement length-scale L_c

$$L_c \; = \; O(1 \; fm) \; , \qquad \alpha_s(L_c^{-2}) \; = O(1) \tag{4}$$

that characterizes the distinction between short-distance ($L \ll L_c$) and long-range ($L \gtrsim L_c$) physics in QCD. In the limit of short distances $L \ll L_c$, where $\alpha_s(L^{-2}) \ll 1$, QCD is well described perturbatively by the usual fundamental Lagrangian $\mathcal{L}_L[A^\mu, \psi, \overline{\psi}]$ in terms of the elementary gluon (A^μ) and quark fields ($\psi, \overline{\psi}$). On the other hand, in the limit of large distances $L \gtrsim L_c$, where $\alpha_s(L^{-2}) \gtrsim 1$, hadronic physics is known to be described well by an effective Lagrangian $\mathcal{L}[\chi, U, U^\dagger]$ which is written in terms of the collective fields χ, $U, U^\dagger$ [27], whose interactions are constrained by the scale and chiral properties of the fundamental QCD Lagrangian [28]. By restricting use of the perturbative regime to physics up to distances $L \lesssim L_c$, and the non-perturbative effective theory to $L > L_c$, we can combine both regimes without double-counting, and obtain an field theory description covering the full range $0 < L < \infty$:

$$\begin{aligned} \mathcal{L}_L[A^\mu, \psi, \chi, U] \; &= \; \mathcal{L}_L[A^\mu, \psi, \overline{\psi}] \; + \; \mathcal{L}[\chi, U, U^\dagger] \\ &= \; -\frac{\kappa_L}{4} \; F_{\mu\nu,a} F_a^{\mu\nu} \; + \; \overline{\psi}_i \Big[\; \Big(i\gamma_\mu \partial^\mu - \mu_L \Big) \delta_{ij} - g_s \gamma_\mu A_a^\mu T_a^{ij} \Big] \; \psi_j \end{aligned}$$

$$+\frac{1}{2}(\partial_\mu\chi)(\partial^\mu\chi) \;+\; \frac{1}{4}Tr\left[(\partial_\mu U)(\partial^\mu U^\dagger)\right] \;-\; V(\chi,U)\,, \qquad (5)$$

where $F_a^{\mu\nu} = \partial^\mu A_a^\nu - \partial^\nu A_a^\mu + g_s f_{abc} A_b^\mu A_c^\nu$, and summation over the color indices a, i,j is understood. The functions κ_L and μ_L introduce an explicit scale(L)-dependence in $\mathcal{L}_L$, which modifies the quark and gluon properties when L increases towards L_c and beyond. In the limit $L \to 0$, $\kappa_L = 1$ and $\mu_L = 0$ (neglecting the quark current masses), and the fundamental QCD Lagrangian is recovered. However, at larger L, the bare quark and gluon fields become dressed by non-perturbative dynamics, and we expect $\kappa_L < 1$ and $\mu_L \neq 0$ [2]. The effective potential $V(\chi,U)$ governs the dynamical interpolation between short- and long-distance domains: at very small L, where the typical distance between color charges is $\ll L_c$, it is equal to the usual QCD vacuum pressure, but as L becomes large due to the expanding spatial separation of color charges, it simulates long-range confinement forces. Explicit expressions for κ_L, μ_L and V can be found in Ref. [20].

2.1.2 Kinetic Equations for Space-Time Evolution

In Ref. [17] it was shown how, under certain assumptions, one can derive from the exact quantum field theory an approximate kinetic theory. Applied to the present case, we formulated in [20] a transport-theory framework that incorporates both partons and hadrons, yielding a fully dynamical description of QCD matter in real time and complete phase-space. Starting from the field equations of motion that follow from (5), we obtained the corresponding Dyson-Schwinger equations for the 2-point Green functions of the fields ψ, A^μ, χ, and U, which measure the time-ordered correlations between the fields at different space-time points. The transition from the quantum-field formulation to a kinetic description was then achieved by relating the Green functions of the elementary partonic fields $(A^\mu, \psi, \overline{\psi})$ and of the collective hadronic degrees of freedom $(\chi, U, U^\dagger)$ to corresponding particle densities F_α for the species $\alpha = p, c, h$ of partons, clusters (prehadronic color-singlets), and hadrons, respectively:

$$F_\alpha(r,k) \;\equiv\; F_\alpha(t,\vec{r};\vec{k},k^2) \;=\; \frac{dN_\alpha(t)}{d^3r\,d^4k}\,, \qquad (6)$$

[2] In fact, the short-range behaviour of κ_L (and similarly of μ_L) can be calculated perturbatively: $\kappa_L = [1 + g_s^2/(8\pi)^2(11 - 2n_f/3)\ln(L\,\Lambda)]^{-1}$. Hence both κ_L and the dynamical quark masses μ_L vary (as does the coupling constant g_s) with the renormalization scale Λ, which we expect to be inversely related to the confinement scale L_c.

which are the quantum-mechanical analogues to the classical phase-space distributions that measure the number of particles at time t in a phase-space element $d^3r d^4k$. The F_α contain the essential microscopic information required for a statistical description of the time-evolution of a many-particle system in complete phase space, and provide the basis for calculating macroscopic observables in the framework of relativistic kinetic theory. In terms of the particle densities (6), the kinetic equations derived from the Dyson-Schwinger equations yield a set of coupled transport equations of the generic form

$$k_\mu \frac{\partial}{\partial r^\mu} F_\alpha(r,k) \;=\; \sum_{processes\ j} \left[\hat{\mathcal{I}}_j^{(+)}(F_\beta) \;-\; \hat{\mathcal{I}}_j^{(-)}(F_\beta) \right] . \tag{7}$$

These kinetic equations reflect a probabilistic interpretation of QCD evolution in terms of successive interaction processes j, in which the rate of change of the particle distributions F_α in a phase-space element $d^3r d^4k$ is governed by the balance of gain (+) and loss (−) terms. On the left-hand side, the covariant operator $k^\mu \partial/\partial r^\mu = k^0 \partial/\partial t - \vec{k}\cdot\partial/\partial\vec{r}$ acting on F_α describes free propagation of a quantum of species α, whereas on the right-hand side the interaction kernels $\hat{\mathcal{I}}^{(\pm)}$ are integral operators that incorporate the effects of the particles' self and mutual interactions, and depend functionally on the different particle densities F_β. In general, the interactions include real and virtual emission, absorption, scattering and coalescence. However, in the present case of e^+e^- collisions, where scattering processes and medium effects are absent, the equations simplify considerably, and the kernels $\hat{\mathcal{I}}$ fall into three categories (c.f. Fig. 1):

(i) parton multiplication through real emission processes on the perturbative level, $q \to q+g$, $g \to q+\bar{q}$, $g \to g+g$;

(ii) parton-cluster formation through 2-parton recombinations [3], $q+\bar{q} \to c_1+c_2$, $g+q \to c+q'$, $g+g \to c_1+c_2$;

(iii) hadron formation through decays of the cluster excitations into final-state hadrons, $c \to h$, $c \to h_1+h_2$.

Whereas the branching processes (i) are the fundamental QCD vertices, the cluster formation possibilities (ii) depend on the specific forms of the functions κ_L and μ_L in the model

[3] This class of processes will be enlarged when color is introduced into our approach in Sec. 2.2 below.

Lagrangian (5), and the cluster decay processes (iii) are modelled on the basis of kinematics and phase-space considerations.

In compact symbolic notation, all interaction kernels in (7) can be expressed as convolutions of the densities of radiating or interacting particles F_β with the specific cross sections $\hat{I}_j$ for the processes j, i.e. $\mathcal{I}_j = \prod_\beta F_\beta \circ \hat{I}_j$, and one arrives at the following closed set of balance equations for the densities of partons F_p, clusters F_c and hadrons F_h:

$$k_\mu \, \partial_r^\mu \, F_p = F_{p'} \circ \hat{I}(p' \to pp'') \; - \; F_p \circ \hat{I}(p \to p'p'') \; - \; F_p \, F_{p'} \circ \hat{I}(pp' \to c) \tag{8}$$

$$k_\mu \, \partial_r^\mu \, F_c = F_p \, F_{p'} \circ \hat{I}(pp' \to c) \; - \; F_c \circ \hat{I}(c \to h) \tag{9}$$

$$k_\mu \, \partial_r^\mu \, F_h = F_c \circ \hat{I}(c \to h) \; . \tag{10}$$

where $k_\mu \partial_r^\mu \equiv k^\mu \partial / \partial r^\mu$, and each of the terms on the right-hand side corresponds to one of the above classes (i)-(iii) of processes, and is proportional to the relevant flux, i.e. the density of particles entering a particular vertex. Each kernel $\mathcal{I}$ includes a sum over contributing subprocesses, and a phase-space integration weighted with the associated subprocess probability distribution of the squared amplitude. We discuss the physical significance of the different kernels in more detail in Sec. 3, and the full forms of eqs. (8)-(10) and the explicit expressions for the kernels are given in Ref. [20].

2.1.3 Calculational Scheme

The set of evolution equations (7) can be solved by real-time simulation in full phase space using the computational methods of Refs. [16, 29]. In Sec. 3 we explain in more detail the physical significance of the calculational scheme for the specific cases of jet evolution in the processes (1) and (2).

The concept of the simulation can be summarized as follows: starting from a given initial state [4] at time $t = 0$, the ensemble of particles is evolved in small time steps, $\Delta t = O(10^{-3} \; fm)$, in coarse-grained 7-dimensional phase-space with cells $\Delta\Omega = \Delta^3 r \Delta^3 k \Delta k^0$. The time discretization is chosen to give an optimum resolution of the particle dynamics in space and energy-momentum. The partons propagate along classical trajectories until they interact, i.e., decay (branching process) or recombine (cluster formation). Similarly,

[4] For example, in the case of e^+e^- annihilation via a virtual photon, the initial parton state consists of a jet-initiating $q\bar{q}$ pair with invariant mass Q and flavor f determined by the probability $w_f = e_f^2 / n_f(Q^2) \sqrt{1 - 4m_f^2/Q^2} \, \theta\left(Q^2 - 4m_f^2\right)$, which accounts for the electromagnetic charge and mass threshold.

the clusters so formed travel along classical paths until they decay into hadrons. The corresponding probabilities and time scales of interactions are sampled stochastically from the relevant probability distributions in the kernels $\hat{I}$ of eq. (8)-(10).

With this concept, one can trace the space-time evolution of the multi-particle system self-consistently: at each time step, any off-shell parton is allowed to decay into daughter partons, with a probability determined by its virtuality and life time (we discuss this in more detail in Sec. 3). Also in each step, every parton and its nearest spatial neighbor are considered as defining a fictious space-time bubble in the vacuum, representing a potential candidate for a 2-parton cluster. The probability for parton-cluster conversion is determined by the bubble action for the Lorentz-invariant distance L between the partons. If the two partons do convert into a cluster within any given time slice, they disappear from that phase-space cell, and the composite cluster appears at their centre-of-mass point, from which it propagates on. Otherwise the partons continue in their shower development until the next time slice. The final decay into hadrons of each cluster formed is simulated analogously, and is determined by kinematics and the available phase space. This cascade evolution is followed until all partons have converted, and all clusters have decayed into final-state hadrons.

In this dynamically-evolving system, the crucial quantity that governs the conversion of partons into clusters and thus the structure of the final hadron state, is the space-time scale $L(r_i, r_j)$, defined by (3), which is the separation between two partons at r_i and r_j, defined by the Lorentz-invariant distance measure

$$\Delta_{ij} \;=\; \sqrt{r_{ij}^{\mu}\, r_{ij,\mu}}\;, \qquad r_{ij} \;=\; r_i \,-\, r_j\;, \tag{11}$$

We identify L with the the distance L_{ij} between parton i and its nearest neighbor j:

$$L(r_i, r_j) \;=\; L_{ij} \;\equiv\; \min(\Delta_{i1}, \ldots, \Delta_{ij}, \ldots, \Delta_{in})\;. \tag{12}$$

If the separation bewteen any given parton and its nearest neighbor approaches the confinement scale L_c, cluster formation becomes increasingly likely, and eventually occurs (c.f. Fig. 2). The dynamics of this cluster formation is described by the kernels $F_i F_j \circ \hat{I}(ij \to c)$ in eqs. (8) and (9), that determine the probability for the coalescence of two partons i, j to form clusters c. It is modelled by a distribution of the form

$$\Pi_{ij\to c} \;=\; \mathcal{C}(L_{ij}) \,\left(\, 1 \,-\, \exp\left(-\Delta F\; L_{ij}\right)\right)\;, \tag{13}$$

where $\mathcal{C}$ modifies the small-L_{ij} behaviour where the exponential form is not appropriate [20], L_{ij} is the 2-parton separation defined by (12), and ΔF is the local change in the free energy of the system that is associated with the conversion of the partons to clusters. The latter is determined by the specific form of the confinement potential V in the model Lagrangian (5). Our previous analysis [20] indicates that we can parametrize the resulting probability density (13) as

$$\Pi_{p_i p_j \to c} \;=\; \begin{cases} 0 & \text{if } L_{ij} \;\leq\; L_0 \\ 1 \;-\; \exp\left(\frac{L_0 - L_{ij}}{L_c - L_{ij}}\right) & \text{if } L_0 \;<\; L_{ij} \;\leq\; L_c \\ 1 & \text{if } L_{ij} \;>\; L_c \end{cases} \quad , \tag{14}$$

where $L_c = 0.8\ fm$ is the value for the confinement length scale that fits best the Bose-Einstein correlation data [20], and $L_0 = 0.6\ fm$. The transition interval $[L_0, L_c]$ arises from the finite, thin-walled potential barrier of the model potential V in (5), that separates the perturbative and hadronic vacua. Its effect is to yield a small, but non-vanishing, probability (14) for partons to convert to clusters while their separation is still smaller, but close to, the confinement length scale L_c, as illustrated in Fig. 2. This scheme separates perturbative parton evolution and non-perturbative confinement dynamics in a self-regulating manner, because in the mean it bounds the partons' virtualities from below:

$$k^2 \;\geq\; \mu_0^2 \;=\; O(L_0^{-2}) \tag{15}$$

so that the condition $\alpha_s(k^2) \leq \alpha_s(\mu_0^2) \ll 1$ is imposed dynamically [5] that clearly defines the notion of a perturbative, dressed parton, as opposed to a non-perturbative clustered parton.

The essential parameter in this description is the confinement scale L_c, defined by (4). This is in principle related to the critical temperature in the finite-temperature QCD phase transition, but is in practice subject to some uncertainty. In Ref. [20] we tested different choices by studying the evolution of hadronic e^+e^- events, and found that the details of the transition are rather insensitive to reasonable variations in L_c. However, the value $L_c = 0.8$

[5] Although this condition determines the mean μ_0 to come out around 1 GeV, statistical fluctuations occur with the distance L_{ij} of two partons i and j in the interval $L_c < L_{ij}^{-1} < \mu_0$, in which case we cut off the parton radiation below μ_0, and let the partons propagate freely without branching, until they eventually coalesce.

fm gives the most favorable description of the Bose-Einstein correlations observed on the Z^0 peak, as well as other experimental data.

This completes the summary of Ref. [20]. We now turn to the extension of our model to take better account of color degrees of freedom.

2.2 Color Degrees of Freedom and Correlations

In our previous description of parton evolution and hadron formation, we did not take explicit account of the color degree of freedom, which is after all the origin of the confinement mechanism. Our Ansatz for confinement picture was based exclusively on the dynamically-evolving space-time separations (12) of nearest-neighbor color charges in the parton cascade, rather than on the details of the color structure of the ensemble of produced gluons, quarks and antiquarks. Our underlying justification for this reasoning was the pre-confinement property [30] of jet evolution in perturbative QCD, according to which the partons emitted during a cascade tend to arrange themselves into a collection of color-singlet systems, which may be viewed as minimal pre-hadronic units. The following two important features characterize the pre-confinement phenomenon [19]. First, the color-singlet subsytems of partons so formed, typically have masses of the order of 1 - 2 GeV, independent of the total energy of the system as a whole. Second, in the leading-logarithmic approximation, the color quantum numbers are naturally ordered in such a way that the partons which form a color singlet are topologically nearby in a cascade (c.f. Fig. 3), and have a finite space-time separation in the color-singlet rest-frame.

It is therefore suggestive to identify these color-singlet systems with the prehadronic clusters in our approach, as we did implicitly in our previous work [20]. It should be emphasized, however, that this correspondence between the color and space-time structures of a parton cascade is not an equivalence, but holds only in the average [2, 31, 32, 33]: whereas the color structure of a cascade tree provides in principle exact microscopic information about the flow of color charges, the space-time structure is based in our model on the statistical kinetic description of parton emission and the nearest-neighbor search, which may be subject to fluctuations that deviate from the exact color flow. This issue becomes increasingly important when more particles populate a phase-space region (possibly already for the small-x region in deep-inelastic scattering, and certainly for hadron-nucleus or heavy-ion collisions). Intuitively, we would expect it then to become increasingly likely

that nearest neighbors in momentum space would not necessarily form a color-singlet. It could also be that the 'natural' color-singlet partner for a given parton within the same cascade (its 'endogamous' partner) might actually be dynamically-disfavoured by comparison with a color-singlet partner from a different, but overlapping, cascade (an 'exogamous' partner). A crucial first step in addressing the latter possibility has been the scenario for 'color reconnection', first explored phenomenologically in [7]. We believe that our model, which is capable of following simultaneously the space-time developments of overlapping cascades, provides a potentially-interesting alternative tool for addressing these issues. Moreover, our nearest-neighbor criterion (12) provides a plausible way of using this tool to resolve questions of 'color reconnection'.

Accordingly we now incorporate color flow into our model, within the general framework of the probabilistic parton cascade description of QCD jets that works so impressively well at high energies (see e.g. [34]). We assign to each parton a color (C) and an anticolor (A) label:

$$(C,\,A) \;=\; \begin{cases} (i,0) & \text{quarks} \\ (0,j) & \text{antiquarks} \\ (k,l) & \text{gluons} \end{cases} \quad , \qquad (i,j,k,l \;=\; 1,\ldots,N_c)\;. \tag{16}$$

It is straightforward to specify the color flow at each elementary vertex for parton branching, and in parton recombinations to form clusters, as shown in Fig. 4 and Fig. 5, respectively. Since it is the nature of a probabilistic description that it only depends on the local properties of the system (i.e. non-local interference effects are assumed to be negligible), this scheme provides an unambigous local tracer of the color flow, in complete analogy to energy-momentum and flavor flow. It is a defect of this approach that there are nine, rather than eight, gluon color states. We have made numerical studies varying N_c, and found no significant effects in our results. However, this point remains a conceptual issue that needs to be thought through more carefully. In particular, it would be desirable to understand the relation of our approach to the $1/N_c$ expansion and the dominance of planar diagrams in high-energy QCD [19].

To see how important color correlations can be, we distinguish the following three scenarios, which differ in their level of accounting for the color flow in conjuction with the space-time evolution.

(I) *Color-Blind* Scenario: The color degrees of freedom (16) are ignored. Cluster formation of partons is based solely on the nearest-neighbor criterion (12). It is assumed that pairs of nearest-neighbor partons are on the average also color-singlets, and therefore can form one, or two pre-hadronic clusters.

(II) *Color-Singlet* Scenario: As (I), but with the additional restriction that the color degrees of freedom (16) of two partons that are potential candidates to form a cluster must add up to a color-singlet combination [6]. This corresponds to considering only the $2 \to 2$ 'color-singlet' processes of the left column in Fig. 5.

(III) *Color-Full* Scenario: No restrictions whatsoever are imposed on the colors of pairs of partons participating in the formation of a cluster, meaning that, in contrast to (II), all the processes illustrated in Fig. 5 are included, i.e. $2 \to 2$, $2 \to 3$, and $2 \to 4$. If the space-time separation (12) of two nearest-neighbor partons allows coalescence, they can always produce one or two color-singlet clusters, accompanied, if necessary, by the emission of a gluon or quark that carries away any unbalanced net color.

We note that the elementary branching processes remain the same as before except for the additional color information, but that the cluster formation dynamics depends on the scenario considered: scenario (I) corresponds to our original approach [20] as reviewed earlier in this Section, scenario (II) is the most restrictive one, in that it allows only a minimal number of processes, whereas scenario (III) is the most diverse, in the sense that it increases the original number of processes by allowing additional parton emission.

In the following Section we compare the application of the three scenarios to e^+e^- events of the types (1) and (2), i.e. via $Z^0 \to 2\ jets$ and $W^+W^- \to 4\ jets$. As we will show, our results for the overall space-time development, as well as for global event measures such as multiplicities or momentum spectra, are rather insensitive to the differences between the above color structure scenarios. However, as we shall see, more sensitive observables may

[6] Color-neutral systems need not be color singlets: for example, the color-octet representation of $SU(3)_c$ contains two color-neutral members, meaning that they possess zero eigenvalues of the non-comuting generators τ_3 and τ_8. In the classical approximation of parton showers, the color phase of the amplitude for each emission is random, so that the final-state partons are statistically distributed among the possible $SU(3)_c$ representations. Therefore, in this naive approximation, e.g., a color-neutral $q\bar{q}$ pair has equal probabilities for being a color singlet or a color octet.

well distinguish between them, in particular the measurement of the W mass in 4-jet events of the type (2).

3. APPLICATION TO HADRONIC e^+e^- EVENTS AT LEP

This Section is devoted to the Monte Carlo simulation of the hadronic e^+e^- event types (1) and (2) within the variants of our model outlined in Sec. 2.1.3. Between 50000 and 150000 events were accumulated in each simulation, depending on the statistical accuracy required for each calculated observable. Each event generated was traced in time steps $\Delta t = 10^{-3}\ fm$ from the decay of the jet-initiating particle (γ^* or Z^0) at $t_0 = 0$, up to a final time $t_f = 20\ fm$ afterwards, when the parton showers have completed their conversion into final-state hadrons.

We study first the case of 2-jet evolution in $e^+e^- \to Z^0 \to hadrons$ on the Z^0 peak at the nominal energy of LEP1, $\sqrt{s} = 91$ GeV, and subsequently the more complex case of 4-jet evolution in $e^+e^- \to W^+W^- \to hadrons$ at the nominal LEP2 energy of $\sqrt{s} = 170$ GeV. We focus particular attention on the following two issues: a) the characteristics of the space-time evolution, which we discuss in the light of the 'inside-outside cascade' picture [25, 32], and b) the impact of color correlations on observable quantities in experiments, comparing the scenarios (I)-(III) defined at the end of the previous Section.

3.1 $e^+e^- \to Z^0 \to q_1\bar{q}_2 \to hadrons$ at $\sqrt{s} = 91$ GeV

Let us return to the kinetic equations (8)-(10) that describe for e^+e^- collisions the cascade evolution of the mixed particle system consisting of gluons, quarks, antiquarks, prehadronic clusters and hadronic states. We discuss the physical significance of the equations and the emerging space-time picture first for the simpler event type (1) of an evolving 2-jet configuration produced by a virtual Z^0. The additional features of the event type (2) are addressed in Sec. 3.2.

3.1.1 General Discussion

Consider the production of the initial quark-antiquark pair $q_1\bar{q}_2$ with opposite flavor and color quantum numbers on the Z^0 peak in the restframe of the decaying Z^0 at an invariant mass $Q = \sqrt{s} = E_{cm}$. Let us for the moment ignore the parton-cluster hadronization

mechanism, and focus on the early stage of parton cascade evolution. In this case only eq. (8) is relevant, and the right-hand side includes solely the space-time version of the leading-log QCD-evolution kernels [20] (the third term would be absent). That implies, initially, free streaming of the initial q_1 and $\bar{q}_2$ which recede back-to-back along straight-line trajectories away from the $Z^0 \to q\bar{q}$ vertex, which we choose as $r_0^{Z^0} := (t_0, \vec{r}_0) = (0, \vec{0})$. Their velocities are $\vec{\beta}_{1,2} = \pm\vec{p}_{cm}/E_{cm}$, where $\vec{p}_{cm} = \vec{k}_1 = -\vec{k}_2$, $E_1 = E_2 = \sqrt{p_{cm}^2 + m_q^2}$. The q_1 and $\bar{q}_2$ are off-shell with a time-like virtuality $k_i^2 < k_{i\,max}^2 = Q^2/4$ $(i = 1, 2)$, and hence live only for a finite time before they decay by gluon emission. In the Z^0 rest-frame, the characteristic life time is [32, 33]

$$t_p(x_i, k_i^2) \;=\; \gamma_i\,\tau_i \;\simeq\; E_i/k_i^2 \;=\; \frac{x_i Q}{2\,k_i^2}\;, \tag{17}$$

where the γ_i are the Lorentz factors of q_1 and $\bar{q}_2$, the $\tau_i \simeq 1/\sqrt{k_i^2}$ their proper life times as given by the uncertainty principle, and the $x_i = E_i/E_{cm} = 2E_i/Q$ their energy fractions. When and where in space time the decays of the $q_i \equiv q_1, \bar{q}_2$ occur is obtained statistically from the kernels $F_{q_i} \circ \hat{I}(q_i \to q_i' g_i'')$ in eq. (8), that incorporate the probability distributions for the branchings of momenta $k_i \to k_i' + k_i''$ with energy ratios $z = x_i'/x_i$ and $1 - z = x_i''/x_i$,

$$\Pi_{q_i \to q_i' g_i''} \;=\; \frac{\alpha_s\left[(1-z)k_i^2\right]}{2\pi}\;\gamma_{q_i \to q_i' g_i''}(z)\;\; T_{q_i}(x_i, k_i^2)\;\;, \tag{18}$$

where the argument of α_s is set by the momentum scale $(1 - z)k_i^2 \approx k_\perp^2$ associated with the vertex [19], the function $\gamma(z)$ denotes the usual DGLAP energy- (z-) distribution [35, 36], and the life-time factor T_{q_i} expresses the probability for the quark or antiquark q_i of virtuality k_i^2 to decay within a time interval Δt in the Z^0 rest-frame,

$$T_{q_i}(x_i, k_i^2) \;=\; 1 \;-\; \exp\left(-\frac{\Delta t}{t_{q_i}(x_i, k_i^2)}\right)\;, \tag{19}$$

where $t_{q_i}(x_i, k_i^2)$ is given by (17).

The daughter partons of the initial branchings $q_1 \to q_1' g_1''$ and $\bar{q}_2 \to \bar{q}_2' g_2''$ then follow the same pattern, with $k_i'^2, k_i''^2 < k_i^2$ and corresponding life times $t(x_i', k_i'^2)$ and $t(x_i'', k_i''^2)$. The elementary branchings that can occur are $q \to qg$, $\bar{q} \to \bar{q}g$, $g \to gg$, $g \to q\bar{q}$. We employ the (modified) leading-logarithmic description [1, 36] in conjunction with the angular ordering [19] of subsequent emissions, which is equivalent to an ordering in virtualities at large x, but accounts for interference effects among soft gluons at small x.

The parton shower thus develops as illustrated in Fig. 6, where the time estimate for the n'th branching is

$$t_n \;=\; \sum_{i=1}^{n} t(x_i, k_i^2) \;=\; \frac{Q}{2} \sum_{i=1}^{n} \frac{x_i}{k_i^2} \,. \tag{20}$$

In the leading-logarithmic approximation and in the limit of small x, these considerations lead to the following analytical result for the average time development of the parton cascade [32]:

$$\langle\, t_p(x, k^2) \rangle \;\sim\; a\, \frac{xQ}{2k^2}\, \exp\left(- b \sqrt{\ln\left(\frac{1}{x}\right)} \right) \,, \tag{21}$$

in the limit $x \ll 1$ and $k^2 \simeq \mu_0^2$, where $\mu_0 \simeq 1$ GeV, and a and b are slowly-varying functions of Q^2 and k^2. Hence, as $x \to 0$, the average time for parton production $\langle t_p \rangle \to 0$, implying that soft (small-x) partons are emitted earlier than the fast (large-x) ones. This fact is a consequence of time dilation, and is known as the 'inside-outside cascade' [25, 26]. We will return to this analytical property when discussing our numerical results below.

Because the virtualities are strongly ordered in the leading-logarithmic approximation, and decrease in a time-like cascade, the quanta become increasingly 'dressed': $k^2 \to \Lambda_{QCD}^2$ as time progresses: $t \to \infty$. In the absence of confinement, they would eventually reach mass shell. However, the confinement length scale L_c, defined by (4), limits the time that the partons can evolve perturbatively, so that they never manage to reach mass shell, but first undergo the non-perturbative hadronization mechanism. It is here that the cluster formation scheme outlined in the previous section terminates locally the perturbative evolution, by coalescing two nearest-neighbor partons i and j, if their separation L_{ij} (12) in their common rest-frame approaches or exceeds L_c (as described before in Sec. 2.1), thereby simulating the screening of the color charges [31, 32], which is responsible for confinement.

Once two partons i and j coalesce, the combined system with invariant mass $m_{ij} \equiv \sqrt{(k_i + k_j)^2}$ is decayed into the outgoing cluster(s) and possible additional partons by using 2- or 3-body decay kinematics and phase-space, depending which of the actual processes of Fig. 5 occurs. In the case of the 2-cluster processes $i + j \to c_1 + c_2$, consistent with the symmetry under exchange of c_1 and c_2, the mass m_c of the first cluster c_1 is sampled from an exponential distribution $\propto \exp[-m_c/(m_{ij} - m_c)]$, and the second cluster c_2 carries off the remaining energy-momentum according to 2-body decay kinematics. An analogous procedure is used for processes with the emission of one parton l, $i+j \to c+l$ by replacing c_2 with l. In the case of a cluster c accompanied by two emitted partons l_1, l_2, $i+j \to c+l_1+l_2$,

again the cluster mass is generated, and then 3-body decay kinematics determines the four-momenta of the two outgoing partons in the rest-frame of $i + j$. In each case, the outgoing particles are then boosted from the $i+j$ rest-frame back to the Z^0 frame. Whereas any outgoing parton participates in the continuing perturbative shower development, each produced cluster with determined four-momentum $k_c^\mu = (E_c, \vec{k}_c)$, mass $m_c = k_c^2$ and proper life time $\tau_c = 1/m_c$, propagates along a straight path with velocity $\vec{k}_c/E_c$ until it converts into final-state hadrons after a life time

$$t_c(E_c, m_c) \;=\; \gamma_c \, \tau_c \;\simeq\; \frac{E_c}{m_c^2} \,, \tag{22}$$

This cluster-decay scheme is embedded in the kernels $F_c \circ \hat{I}(c \to h)$ of eqs. (9) and (10), and is modelled [20] along the lines originally proposed in [37]: If a cluster is too light to decay into a pair of hadrons, it is taken to represent the lightest single meson that corresponds to its partonic constituents. Otherwise, the cluster decays isotropically in its rest-frame into a pair of hadrons, either mesons or baryons, whose combined quantum numbers correspond to its partonic constituents. The corresponding decay probability is chosen to be

$$\Pi_{c\to h} \;=\; T_c(E_c, m_c^2) \;\; \mathcal{N} \int_{m_h}^{m_c} \frac{dm}{m^3} \; \exp\left(-\frac{m}{m_0}\right) \,, \tag{23}$$

where $\mathcal{N}$ is a normalization factor, and the integrand is a Hagedorn spectrum [38] that parametrizes quite well the density of accessible hadronic states below m_c which are listed in the particle data tables, and $m_0 \simeq m_\pi$. In analogy to (19), T_c is a life-time factor giving the probability that a cluster of mass m_c^2 decays within a time interval Δt in the Z^0 rest-frame

$$T_c(E_c, m_c^2) \;=\; 1 \;-\; \exp\left(-\frac{\Delta t}{t_c(E_c, m_c^2)}\right) \,, \tag{24}$$

with the Lorentz-boosted life time $t_c(E_c, M_c^2)$ given by (22). The only exception to the above rules is that if a cluster is very heavy, $m_c > m_{fiss} = 4$ GeV, it undergoes one or more fissions before the products then decay into hadron pairs [37, 20]. In this scheme, a particular cluster decay mode is obtained from (23) by summing over all possible decay channels, weighted with the appropriate spin, flavor, and phase-space factors, and then choosing the actual decay mode acording to the relative probabilities of the channels.

In summary, we perform a complete simulation of the collision process which follows the microscopic space-time development from the initial $q\bar{q}$ of the Z^0 decay, via parton-shower

evolution and parton-cluster formation and decay, all the way to the final-state hadrons. The origins of all the hadronic observables are therefore recorded in the particular space-time history of the system.

3.1.2 Numerical Results

We now discuss the results of our numerical simulations for e^+e^- collisions at 91 GeV, paying particular attention to the comparison between the color scenarios (I)-(III) defined in Sec. 2.2. We chose for each of these scenarios an appropriate value for the minimum required parton virtuality during the cascade evolution, μ_0 of (15), so as to reproduce the *charged* multiplicity, which is determined quite accurately by experiment: $n_{ch} = 20.95 \pm 0.88$ [3]. Table 1 summarizes the values for μ_0 required by this procedure, as well as the calculated multiplicities of partons and hadrons, which are compared with with experimental data [21] where available. One observes that the color-blind scenario (I) requires the smallest value of μ_0, whereas the color-full scenario (III) needs the largest value. Correpondingly, the parton multiplicities are largest (smallest) in these two extreme scenarios. However, the *total* hadron multiplicity does not follow the same pattern, since scenario (III) produces the largest yield, giving the smallest parton-to-hadron ratio. This is due to the presence of cluster-formation processes involving additional parton emission, which lead in the average to lower-mass clusters, because the emitted parton(s) take away energy-momentum. Since the total energy of the system is conserved, in the end a larger number of clusters with lower mean masses are been produced (c.f. Table 2), which leads naturally to an increase of the hadron multiplicity. Regarding the individual hadron multiplicities, there are significant differences between scenarios (I)-(III) in the particle composition of the final state, but the numbers are generally within reasonable range of the available experimental data, even in the absence of further tuning of the scenarios.

Fig. 7 reflects the emerging time-evolution pattern of the dynamical development of the mixed-particle system, presenting more details of the parton showering and of parton-hadron conversion. The four plots show the relative proportions of partons and hadrons, the conversion of the total energy, the fractions that the partons and hadrons carry of the longitudinal momentum fractions along the 2-jet axis, and the total produced transverse momentum perpendicular to this axis. One can conclude, first, that the evolution can be divided crudely into three stages: (i) a *parton shower stage* ($\lesssim 0.5\ fm$), (ii) a *parton-hadron*

conversion stage ($\approx 0.5 - 5\ fm$), and, (iii) a *hadron stage* ($\gtrsim 5\ fm$). Second, it is evident that at a macroscopic level the overall space-time evolution is only marginally different for scenarios (I)-(III), implying that the gross features of the dynamical parton-hadron conversion are primarily determined by kinematics and the way in which the particles occupy phase space, and to a much lesser extent by the role of the internal color degrees of freedom.

Fig. 8 shows that the differences among the color flow scenarios (I)-(III) have a particularly small impact on the resulting cluster size- and mass-spectra, as well as on the momentum distributions of the hadrons that emerge from the cluster decays. This is also reflected in the cluster properties listed in Table 2, which supplements the previous Table 1. Table 2 provides, in addition, a listing of the relative contributions of the various parton-cluster formation processes defined in Fig. 5. Comparing the color-singlet and color-full scenarios (II) and (III), respectively, one may conclude that most processes in the latter case are of non-singlet type, accompanied by color emission. On the other hand, scenarios (I) and (III) give very similar total rates for gg, $q\bar{q}$ and qg cluster processes, whereas scenario (II) clearly differs. It is the most restrictive in the sense that it allows only color-singlet clustering, and consequently suppresses substantially direct gg or $q\bar{q}$ recombinations, because the color non-singlet configurations among these are vetoed. This yields an increase of the relative qg recombination rate, since here the outgoing quark can carry off the net color.

The conclusion from these results is that global quantities associated with the bulk multi-particle system, averaged over many events, do not exhibit obvious spectacular effects of the color flow structure. In order to extract an observable effect, one has to study particular event shapes or other measures that are sensitive to the local color structure of the system. In the next Section we give examples in the context of the W mass determination in events of the type (2), and find significantly distinct results.

Before doing so, however, we return to the general space-time structure of the event evolution, and explore whether our approach is consistent with the 'inside-outside' cascade picture that one expects from both intuitive considerations [25, 26] and the formal arguments [31, 32] reviewed earlier. We see in Figs. 9 and 10 that the answer is 'yes'. In Fig. 9 we show the time developments of the parton spectra versus rapidity y, longitudi-

nal direction z along the 2-jet axis, transverse momentum $p_\perp$, and perpendicular direction $r_\perp$. In Fig. 10, the corresponding time developments of the hadron spectra are plotted. The various curves correspond to 'snapshots' taken during the course of the evolution at the indicated discrete time intervals in the Z^0 rest-frame. The simulations clearly exhibit the expected 'inside-outside' character of the rapidity (y) and longitudinal (z) space-time evolution. The central y- and z-region is populated the earliest, first by the bulk of small-x partons with [7] $y \simeq \ln x$, and then by hadrons that result from the disappearing partons in the cluster formation process. This property is in accord with the perturbative QCD result (21) calculated in the leading-logarithmic approximation. The regions at larger y and z are gradually populated later, as the system expands. Furthermore, one sees that the time-development in transverse momentum- and coordinate-space proceeds by diffusion in both $p_\perp$ and $r_\perp$. The average absolute value of $p_\perp$ per particle decreases (although the total transverse momentum grows, c.f. Fig. 7), and so the slope of the distribution steepens with progressing time. This is a random walk effect, which is mirrored in the diffusion in $r_\perp$ with a broadening particle population prependicular to the jet axis.

Finally, Fig. 11 gives a 2-dimensional visualization of this 'inside-outside' picture in $log(t)$ versus y (top), and z (bottom). We show the particle ratios

$$R_{y,z}(t) \;=\; \frac{\rho^{(h)}_{y,z}}{\rho^{(p)}_{y,z} + \rho^{(h)}_{y,z}} \;, \tag{25}$$

where

$$\rho^{(p,h)}_{y} \;\equiv\; \frac{dN^{(p,h)}(t)}{dy} \;, \qquad \rho^{(p,h)}_{z} \;\equiv\; \frac{dN^{(p,h)}(t)}{dz} \;, \tag{26}$$

i.e., the number of hadrons divided by the total number of particles, which measures the rate of hadron yield locally in y and z. Initially zero, the ratios (25) must approach unity as time progresses. The plots again confirm that time dilation from the particles' local, comoving frame to the Z^0 rest-frame yields a picture in which hadrons are first produced at small y and z where most partons are emitted at early time, and then 'eat' their way out to larger rapidity and spatial distance from the initial Z^0 vertex.

3.2. $e^+e^- \to \gamma^*/Z^0 \to W^+W^- \to q_1\bar{q}_2q_3\bar{q}_4 \to$ *hadrons* at $\sqrt{s} = 170$ GeV

[7] The general relation between rapidity y and energy (or momentum) fraction x is $y = -\ln(1/x) - 1/2\,\ln((k^2+k_\perp^2)/Q^2)$, which implies approximately $y \simeq |\ln x|$ for sufficiently large k^2.

The 4-jet evolution initiated by the $q\bar{q}$ decays of a W^+ and a W^- that were produced by an intermediate γ^* or Z^0 embodies new features compared to the previous case of 2-jet evolution of a single $q\bar{q}$-pair. In particular, since the W^+ and W^- decay vertices overlap in space, the initial state is a single QCD "hot spot" in which collective non-perturbative hadronization effects can be important. We proceed as in the preceding Section, by discussing first the general space-time picture of the process, proceeding later to investigate the different color correlation effects in scenarios (I)-(III), with an eye to the experimental measurement of the W mass through jet reconstruction.

3.2.1 General Discussion

Again we describe the dynamics in the overall center-of-mass frame, that is the rest-frame of the γ^*/Z^0 with invariant mass $Q = E_{cm} = \sqrt{s}$. The produced W^+ and W^- are generally off mass shell, meaning that their masses $m^\pm$ are unequal, and differ from the nominal on-shell value, which we take to be $m_W = 80.22$ GeV [39]. The distribution of produced masses $m^\pm$ can be described by a relativistic Breit-Wigner distribution,

$$\Pi(m^\pm) \;=\; const.\; \frac{(\Gamma_W/m_W)^2}{1-(m_W/m^\pm)^2 \;+\; (\Gamma_W/m_W)^2}\;, \tag{27}$$

where the full width is taken to be $\Gamma_W = 2.12$ GeV [39]. As a consequence, the energies $E^\pm = (s \pm ((m^+)^2 - (m^-)^2)/\sqrt{4s}$ differ from those expected in the naive on-mass-shell case where $m^+ = m^- = m_W$. Furthermore, although the three-momenta satisfy $\vec{p}^{\,+} = -\vec{p}^{\,-}$, the cm-momentum $p_{cm} \equiv |\vec{p}^{\,+}| = |\vec{p}^{\,-}|$ deviates [8] from the naive case: in fact, $p_{cm} \simeq 20$ GeV at $\sqrt{s} = 2m_W \simeq 160$ GeV, rather than the naive value $p_{cm}^{naive} = 0$, and $p_{cm} \simeq 30$ GeV at $\sqrt{s} = 170$ GeV.

With this kinematic situation in mind, we describe the evolution of the system as follows. As before, we choose the space-time position of the γ^*/Z^0-decay vertex to be $r_0^{\gamma^*/Z^0} := (t_0, \vec{r}_0) = (0, \vec{0})$. The produced W^+ and W^- recede in opposite directions with different velocities $\vec{\beta}^\pm = \pm\vec{p}_{cm}/E^\pm$, and different Lorentz boost factors $\gamma^\pm = E^\pm/m^\pm$. This causes variations in the life times of the W^+ and W^- in the center-of-mass frame:

$$\langle\, t^\pm \,\rangle \;=\; \gamma^\pm\, \tau^\pm \tag{28}$$

and the two particles subsequently decay at space-time vertices separated by

$$r^\pm \;\equiv\; (t^\pm, \vec{r}^{\,\pm}) \;=\; \gamma^\pm \tau^\pm\, (1, \vec{\beta}^\pm) \tag{29}$$

from $r_0^{Z^0} = (0, \vec{0})$. The proper life times $\tau^{\pm}$ are given by a distribution

$$\Pi(\tau^{\pm}) \;=\; \frac{1}{\tau_W(m^{\pm})}\;\exp\left(-\frac{\tau^{\pm}}{\tau_W(m^{\pm})}\right) \tag{30}$$

with [8]

$$\tau_W(m^{\pm}) \;=\; \frac{m^{\pm}}{\sqrt{(m^{\pm\,2} - m_W^2)^2 \;+\; (\Gamma_W\, m^{\pm\,2}/m_W)^2}}\;. \tag{31}$$

Because of the short proper life time resulting from (31), and the fact that the boost factors are not large near the W^+W^- threshold at the nominal LEP2 energy of $\sqrt{s} = 170$ GeV, the vertices are typically very close [8]: on the average, the time separation is $|t^+ - t^-| \simeq 0.08$ fm and the spatial separation is $|\vec{r}^{\,+} - \vec{r}^{\,-}| \simeq 0.05$ fm. This situation is illustrated in Fig. 12, which is meant to represent the creation of a single QCD "hot spot", rather than of two independent "hot spots".

The W^+ and W^- each decay into a time-like $q\bar{q}$-pair, and both the $q_1\bar{q}_2$ and the $q_3\bar{q}_4$ are produced off-shell with maximum virtualities $k^2_{1,2} < (m^+)^2/4$ and $k^2_{3,4} < (m^-)^2/4$. Assuming that perturbative interference effects between the W^+ and W^- decays are negligible [8], we then visualize each $q\bar{q}$-pair as a 2-jet system that initiates an independent time-like parton shower, whose evolution we describe in coherent angular-ordered manner using the same scheme as in the previous Section: the two cascades develop by successive parton emission, followed by cluster formation and final cluster decay into hadrons. There is, however, an important physical difference as compared to the case of a single 2-jet evolution. Due to the close proximity of the initial $q_1\bar{q}_2$ and $q_3\bar{q}_4$ pairs, the associated 2-jet systems overlap in space-time, which results in overlapping phase-space populations from the two showers, implying that parton correlations are likely to affect the recombination of partons to color-singlet clusters, and hence the hadron yield. This leads to a mixing of the individual cascades initiated by the initial $q_1\bar{q}_2$ and $q_3\bar{q}_4$ pairs, which effaces the original identity of the jets, at least in the central low-momentum (-rapidity) region. The effect is especially important here because, as is clear from the discussion in Sec. 3.1, the bulk of parton emissions occurs at very early times, while the $W^{\pm}$ showers are still overlapping, and at small energy fractions x. Therefore one would expect within our parton-cluster formation scheme, which is based on the nearest-neighbor separation of a given pair of

[8] As has been noted in [8], this expression, which follows from the assumed Breit-Wigner distribution (27), is not exact. A general discussion of unstable particle life-times can be found in, e.g., Ref. [40].

partons in conjunction with their color combination, that locally the number of possible 2-parton combinations would be significantly increased to include many possible 'exogamous' partnerships between a parton originating from one 2-jet system and a parton from the other 2-jet system. The enhanced cluster formation possibilities should then be mirrored in the hadronic mass spectrum, because the cluster-hadron decays are described as local, independent processes. In our analysis, there is no mechanism for suppressing 'exogamy' relative to the normal assumption of 'endogamy', according to which only partons from the same 2-jet system can coalesce, with the exception of some limited amount of 'color reconnection' [8]. We will return to these issues below, when we present numerical results which confirm these effects.

3.2.2 Numerical Results

We have used in our numerical simulations of W^+W^- production at the nominal LEP2 energy of 170 GeV the values of the parameters L_c, L_0, μ_0 that we specified in Sec. 3.1, on our discussion of Z^0 decays at LEP1. To study within our framework whether the spatial overlap of parton production from the W^+ and W^- decays results in observable effects, we contrast two extreme sets of initial conditions for the production of W^+W^- pairs:

a) the *realistic* case, in which the W^+ and W^- decay close by at space-time vertices $r^{\pm}$, eq. (29), with an average separation $\Delta r < 0.1\ fm$, and with the spatial correlations between the two jet systems taken fully into account, and

b) a *hypothetical* one with the W^+ and W^- decay vertices shifted artificially apart, i.e. $\Delta r \to \infty$, so that spatial correlations between the two jet systems are absent.

Fig. 13 exhibits the differences between the *realistic* (full curves) and the *hypothetical* (dotted curves) cases for the cluster mass spectrum, the transverse momenta of the produced hadrons, and the multiplicity distribution for charged particles. In both cases, we show results for the 'color-full' coalescence scenario (III) are shown, where the effects are most significant. The main effects of particle correlations in the *realistic* scenario due to the spatial overlap of the jets during the time-development of the system is are seen to be (i) a suppression of cluster production for masses $m_c \gtrsim 2$ GeV, (ii) a softer $p_\perp$-spectrum of resulting hadrons, and (iii) a significantly shifted multiplicity distribution, with an enhanced number of high-multiplicity events and a mean $\langle n_{ch} \rangle = 37.5$ (30.8 in $|y| < 1$), compared to

$\langle n_{ch} \rangle = 32.8$ (25.6 in $|y| < 1$) in the *hypothetical* scenario. This shows that multi-particle effects may well not be negligible. In particular, the difference of more than 10 % in the particle multiplicity between the two sets of initial conditions, which rises to above 20 % in the central rapidity region $|y| < 1$, should be clearly visible at LEP2. If seen, such an effect would enable experimentalists to probe this possible multi-particle situation in more detail, This would in turn enable our simulation to be improved and extended to more complicated cases of overlapping cascades, such as appear, for example, in collisions involving nuclei.

Returning to the three color scenarios (I)-(III) defined in Sec. 2.2, the next question is the extent to which they differ in their predictions for the gross features shown in Fig. 13. Table 3 summarizes for each of the three scenarios our results for particle multplicities and average event properties, including the transverse momenta of the charged particles $\langle p_\perp^{ch} \rangle$, the charged energy fraction $\langle x_E^{ch} \rangle$ and the thrust $\langle T \rangle$. Here $T = \sum_i |p_{\parallel\, i}| / \sum_i |\vec{p}_i|$, with $\vec{p}_i$ the three-momentum of particle i and $p_{\parallel\, i}$ its longitudinal momentum along the axis which maximizes this ratio: T measures the 'jettiness' in the sense that $T = 1$ for a perfect back-to-back configuration and $T = 1/2$ for an isotropic event. Compared with the analogous Table 1 of Sec. 3.1, the outcome is, not surprisingly, very similar. The previously fixed values of μ_0 are the only constraint on the particle production in each of the color scenarios. For the reasons discussed before, again the color-blind scenario (I) gives the largest parton multiplicity but the smallest total number of final hadrons, whereas the color-full scenario (III) features significantly less perturbative parton production, but the largest total hadron multiplicity. Table 4 lists some properties of the cluster formation scheme related to the parton and hadron content. Compared with the corresponding Table 2 of Sec. 3.1, one sees that the ratio between partons and clusters, and between clusters and hadrons, as well as the mean cluster size and radius, are roughly the same for both event types (1) and (2). This implies that the formation and hadronization of the clusters are rather universal and largely independent of the total energy of the system, a result that is plausible, given that our approach works locally in space-time and therefore is insensitive to global properties of the system. Concerning the relative contributions of the various 2-parton cluster formations, as before in Table 1, most processes in the color-full scenario (III) are of non-color-singlet types, and hence accompanied by colored parton emission. For this reason, and since we consider scenario (III) to be the most complete one, we infer

that the color-singlet scenario (II) may not always be reliable. Overall however, all three scenarios give rather similar predictions for these global event properties, so we now proceed to examine more sensitive quantities.

At LEP2, the W mass is one quantity which is of great physics interest and which is also potentially among the most sensitive to particle- and color-correlations. As already explained, we expect the apparent W mass to depend in a non-trivial way on the space-time history of the system, the color stucture of the evolution, and on all particle momenta. It will be an experimental challenge to measure the W mass accurately using jet reconstruction. If the measured jets could be correctly separated, so that each final-state particle could be assigned unambiguously to the decay of either the W^+ or the W^-, then the four-momenta of W^+ and W^- could be reconstructed to give the $W^\pm$ masses. However, as has been pointed out in Ref. [8], in practice such an analysis faces several complications in addition to purely statistical errors, such as the removal of background events, mistakes or ambiguities in assigning individual particles to jets, missing particles and other problems of a technical nature. We will not address these here, but discuss in the following only the physical effects on the W mass determination due to particle- and color-correlations during the QCD evolution of the combined W^+W^- system. In view of the experimental goal at LEP2 of measuring m_W with ≈ 50 MeV accuracy, any physical effect that induces a mass-shift significantly larger than about 100 MeV, compared to the nominal experimental value of 80.22 GeV, is of great importance, as would be any apparent broadening of the Breit-Wigner mass distribution (27). Such a shift and broadening could be caused by ambiguous assignments, or even misassignment [9], of some of the measured particles between the original W^+ and W^-. In particular, within any approach to cluster formation which allows for 'exogamous' coalescence, such as ours, it is not even possible in principle to assign all final-state hadrons unambiguously to one W or the other. Since, as discussed earlier, the spatial overlap between the decay products of the W^+ and W^- is almost perfect, the only natural scale for the net effect on the reconstructed average mass $\overline{m}_W = (m^+ + m^-)/2$ is the QCD energy scale Λ_{QCD}, which is several hundred MeV. To gauge the possible magnitude

[9] The direction of any such effective mass shift is not obvious *a priori*. However, a 'randomization' effect due to experimental misassignment of particles, i.e. attributing hadrons to one W that in fact 'belong' to the other one, would presumably cause an upward shift in general.

of this effect, we compare the *realistic* case of overlapping W production and decay with the *hypothetical* case of far-separated W pairs that we introduced earlier in this Subsection.

In order to obtain an estimate of the possible change in the W mass spectrum due to the increased particle density and the color structure of the parton-cluster conversion, we have simulated, for each of the three scenarios (I)-(III) of Sec. 2.2, the experimental jet reconstruction procedure and the subsequent determination of m_W. We assume that all particles are perfectly measured, so that our analysis exhibits only the physical smearing of the separate identities of the W^+ and W^- associated with the correlation effects of overlapping cascades. To model the experimental reconstruction of the four jets initiated by the W^+ and W^- decays from the observed final-state hadrons, we have adopted the e^+e^- jet-finding algorithm of the JETSET program [22], which is frequently used in experimental analyses. The general purpose of this algorithm is to determine the individual jet axes in events with multiple jets ($n_{jet} > 2$) by grouping together measured particles which are near by in phase space, and then identifying each well-separated group of particles as a jet with the jet axis given by the constituent particle directions. Other jet-finding programs exist, such as the JADE [41] or the Durham [42] algorithms, which are conceptually very similar. Specifically, in the JETSET algorithm a jet is defined as a collection of particles that have a limited transverse momentum with respect to a common jet axis, and hence also with respect to each other. A momentum distance measure d_{ij} is introduced which essentially measures the relative transverse momentum of two particles with momenta $\vec{p}_i$ and $\vec{p}_j$,

$$d_{ij} \;:=\; \frac{4|\vec{p}_i|^2|\vec{p}_j|^2\ \sin^2(\theta_{ij}/2)}{(|\vec{p}_i| + |\vec{p}_j|)^2}\ . \tag{32}$$

A jet is reconstructed by first searching for the highest-momentum particle i, and then all particles j that are within a distance $d_{ij} < d_{max}$ around it. Here the parameter d_{max} is the transverse momentum 'jet resolution power', which depends on the experimental situation and should be chosen such that the identities of the jets found are well separated. In our case, we required a minimum of four jets to be reconstructed, and have found that a value $d_{max} = 10$ GeV satisfies this criterion appropriately. Events that yielded five or more reconstructed jets (about 20 %) were ignored in the following analysis. Furthermore, for the W mass determination we followed the suggestion of Ref. [8] and required that each

jet has an energy of at least 20 GeV, and that the angle between any pair of jets should be larger than 1/2 radian. In agreement with previous studies, we found that about 60 % of the total number of simulated events satisfy these cuts, so that the reconstruction gives four well-separated jets.

The four jets, corresponding to the initially-produced $q_1, \bar{q}_2, q_3, \bar{q}_4$ (c.f. Fig.12), may be paired into a candidate W in three different ways to be associated with the W^+ and W^-, so that each event gives three different values for the reconstructed mass $\overline{m}_W$. To select the most likely pair configuration, we exploit our knowledge of the initial $q_1, \bar{q}_2, q_3, \bar{q}_4$ configuration and map the four reconstructed jets one-to-one to the original partons. Out of the three possible permutations, we then pick the one that minimizes the product of the invariant masses between each jet and the parton. Formally the selection criterion is given by:

$$\Sigma^{(4-jet)} \;:=\; \min\left[\,\mathrm{Perm}_{i,j,k,l}\left\{\,M(i,1)\;M(j,2)\;M(k,3)\;M(l,4)\right\}\right]\;, \tag{33}$$

where

$$M(i,j) \;=\; \sqrt{\left(k_i^{(jet)} \;+\; k_j^{(q)}\right)^2}\;. \tag{34}$$

From the total energy-momentum of the jet pairs selected in this way, one then obtains the two invariant masses m^+ and m^- of the W^+ and W^- and finally the average $\overline{m}_W = (m^+ + m^-)/2$.

We recall that this standard procedure is formulated entirely in momentum space, because the experimental measurements of particle momenta do not yield any explicit information about the spatial distribution or the time of production. However, in view of the close relation between the space-time evolution of the particle system and the emergence of hadrons in momentum space (c.f. Figs. 9-11 and the discussion in Sec.3.1), one can presume that the above jet reconstruction scheme gives a reasonable image of the true jet structure and its underlying space-time history. In particular, since the momentum distance d_{ij} of two particles projects out their relative transverse momentum, and is insensitive to their longitudinal momenta, this distance measure provides a local criterion which is independent of rapidity.

Fig. 14 exhibits rather vividly the differences between our color scenarios (I)-(III) in the jet reconstruction procedure. We plot the mass spectrum of the four reconstructed jets in each W^+W^- event, and the quantity $X := \sum_i^4 |\vec{p}_i^{\,jet}| / \sum_j^n |\vec{p}_j^{\,par}|$, measuring the

fraction of summed jet three-momenta relative to the total three-momentum carried by the whole ensemble of final particles. For both quantities, the color-blind scenario (I), which is solely based on the space-time structure, deviates clearly from the scenarios (II) and (III), which in addition take into account the color structure in the parton-cluster formation processes. As compared to the latter two, which give relatively similar results, scenario (I) is characterized by jets that have, typically, lower mass and larger $\langle X \rangle$.

In Fig. 15 we show our final result for the simulation of the experimental W mass reconstruction. The top part shows the distribution of the reconstructed m_W for each of the color scenarios (I)-(III), in comparison to the W mass distribution which was initially generated and corresponds to the Breit-Wigner spectrum (27). We remark that the average value of the latter is $\langle m_W^{(generated)} \rangle = 79.75$ GeV, and hence below the nominal 'on-shell' value 80.22 GeV, because of the kinematic competition between the Breit-Wigner line shapes of the W^+ and W^- and the phase-space available for production of the pair. As in Fig. 14, the color-blind scenario (I) sticks out significantly also in Fig. 15, whereas the color-singlet and color full scenarios, (II) and (III) give almost identical results. The lower part of Fig. 15 amplifies this effect, by showing the effective mass shift

$$\Delta m_W \;=\; m_W^{(generated)} \;-\; m_W^{(reconstructed)} \;. \tag{35}$$

The mean values of the distributions are

$$\langle\, \Delta m_W \,\rangle_{real}^{(i)} \;=\; \begin{cases} +383 \text{ MeV} & \text{for } i = \text{I} \\ +812 \text{ MeV} & \text{for } i = \text{II} \\ +706 \text{ MeV} & \text{for } i = \text{III} \end{cases} \;. \tag{36}$$

where the subscript 'real' stands for the *realistic* case of spatially-overlapping $W^{\pm}$ decays, as defined above. The widths associated with the Δm_W-distributions are large: $\sigma(\Delta m_W) =$ 2.65/3.05/3.02 GeV for scenarios (I)/(II)/(III), but the effect of the wide tails is presumably not of significance, since any fine-tuned experimental W mass analysis would be mostly sensitive to the peak.

A large shift $\langle \Delta m_W \rangle_{real}$ would not be a problem for measuring the W mass if it were independent of the hadronization model. However, a notable aspect of (36) is the difference in mass shift among the three color scenarios. Defining $\delta m_W^{(II,III)}$ as the difference between the scenarios which incorporate some color-accounting, namely (II) and (III), and the sce-

nario without color, namely (I), this relative mass shift reflects the net effect of particle correlations due to color structure. It turns out to be impressively large:

$$\langle\, \delta m_W \,\rangle^{(i)}_{real} \;\equiv\; \langle\, \Delta m_W \,\rangle^{(i)}_{real} \;-\; \langle\, \Delta m_W \,\rangle^{(I)}_{real} \;=\; \begin{cases} 429 \text{ MeV} & \text{for } i = \text{II} \\ 323 \text{ MeV} & \text{for } i = \text{III} \end{cases} \quad . \tag{37}$$

The differences between the three color scenarios are certainly not negligible compared with the experimental goal of measuring m_W with an accuracy of about 50 MeV. Even the difference between our favored 'color-full' scenario (III) and the next-best scenario (II) in (37),

$$\langle \delta m_W \rangle^{(III)}_{real} - \langle \delta m_W \rangle^{(II)}_{real} \;\simeq\; -100 \text{ MeV} \,, \tag{38}$$

is large compared with this experimental goal.

The mass shifts in (36) and (37) include a mixture of two effects: first,the misassignment of particles to one W that belong in reality to the other, and second, the forced assignment of hadrons to one W that emerged from clusters formed by 'exogamous' pairs of partons with mixed origins from the two overlapping W decays. Some information on the relative contribution of these independent effects can be opbtained by comparing the W mass shift in the above *realistic* case with very near-by $W^{\pm}$ decay vertices (where both misassignments and 'exogamous' clustering are possible), and the *hypothetical* situation with infinitely separated $W^{\pm}$ decay vertices (where 'exogamy' is impossible, but misassignments are still possible). Experimentally, the hypothetical case of widely-separated $W^{\pm}$ decays can be simulated by superposing the decays of a pair of Lorentz-boosted Z^0 decays measured at LEP1, which should enable the *hypothetical* mass shift $\langle \Delta m_W \rangle_{hypo}$ to be understood with adequate precision (~ 10 MeV). It should be noted, though, that misassignment may occur at different rates in the *realistic* and *hypothetical* cases, because of the differences in the final hadron spectra even for 'endogamous' production. We find in the *hypothetical* case the mass shifts

$$\langle\, \Delta m_W \,\rangle^{(i)}_{hypo} \;=\; \begin{cases} +396 \text{ MeV} & \text{for } i = \text{I} \\ +781 \text{ MeV} & \text{for } i = \text{II} \\ +424 \text{ MeV} & \text{for } i = \text{III} \end{cases} \,, \tag{39}$$

compared to the mass shifts (36) in the *realistic* situation. Table 5 gives a comparative list of the various mass shifts in the different cases. Taking the differences, we infer that

hadrons produced 'exogamously' are directly responsible for shifts,

$$\langle\, \Delta m_W \,\rangle^{(i)}_{real} \;-\; \langle\, \Delta m_W \,\rangle^{(i)}_{hypo} \;=\; \begin{cases} -13 \text{ MeV} & \text{for } i = \text{I} \\ +6 \text{ MeV} & \text{for } i = \text{II} \\ +282 \text{ MeV} & \text{for } i = \text{III} \end{cases} \quad . \tag{40}$$

In the absence of a more appropriate comparison, we can only regard the difference between the last two entries in (40), provisionally, as a conservative estimate [10] of the error in determining m_W from purely-hadronic W^+W^- final states.

It should be emphasized that, in the discussion of the previous paragraph, we have been incorporating theoretical knowledge not available to experiments at LEP2, namely the energy-momentum vectors of the initially-produced partons $q_1, \bar{q}_2, q_3, \bar{q}_4$ configuration, which we exploited to remove the jet assignment ambiguity via the criterion (33). In reality this knowledge is absent, so that some other criterion must be found for assigning the four observed jets to the $W^{\pm}$. A systematic study of possible criteria for assigning the four observed jets to the $W^{\pm}$ and W^- involves experimental detector characteristics, and lies beyond the scope of this paper. However, to assure the reader that our results are not dependent on the details of the reconstruction method, but in fact reflect the underlying simulated particle dynamics, we repeated the W mass analysis using an alternative criterion that makes no *a priori* use of knowledge of the initial parton configuration as (33), but solely relies on the final particle momenta. Instead of (33) we picked out of the three possible pair configuration of the four reconstructed jets the one that minimizes the difference between the jet masses and the nominal W mass value $m_W = 80.22$ GeV that we introduced before:

$$\widetilde{\Sigma}^{(4-jet)} \;:=\; \min\left[\text{Perm}_{i,j,k,l} \left\{ \left| \widetilde{M}(i,j) \;-\; m_W \right| \;+\; \left| \widetilde{M}(k,l) \;-\; m_W \right| \right\} \right] \;, \tag{41}$$

where

$$\widetilde{M}(i,j) \;=\; \sqrt{\left(k_i^{(jet)} \;+\; k_j^{(jet)} \right)^2} \,. \tag{42}$$

Using this more experimental reconstruction scheme, we obtain results very similar to those in (36) and (37). Table 5 compares the outcome of the two different reconstruction schemes (33) and (41). From this it is evident, that the latter, more experimental scheme gives

[10] We find qualitatively similar numbers for the mass shifts if we select events with dijet masses in the nighborhood of m_W.

results with a spread similar to those in (40) above. Further study of the magnitude of the particle- and color-correlations will require more detailed experimental simulations.

Although we believe that the 'color-full' scenario (III) is the most reliable, prudence demands that one consider the differences between this and the other scenarios as estimates of the possible systematic error in the determination of m_W, until deeper understanding of the model-dependence of the mass determination is available. For example, one issue, which lies beyond the scope of this paper, is the effect of Bose-Einstein correlations [8, 43]. An alternative way of thinking about the above results would be to take the value of m_W from elsewhere (e.g., from $W^+W^- \to l\,\nu\,q\bar{q}$), and regard hadronic W pairs as a laboratory for studying the effects of space-time and color correlations in a controlled environment. However, we are reluctant to retreat to this position until more model studies and comparisons have been made. We comment on these questions in the final section of this paper, discussing in particular why our result for the shift $\langle \delta m_W \rangle$ is up to an order of magnitude larger than the previous estimates of mass shifts due to color correlations within the 'color reconnection' approach [8, 9, 10, 11, 12].

4. DISCUSSION AND COMPARISON WITH PREVIOUS WORK

In this work we have focussed on two issues of fundamental interest for general high-energy particle collisions in QCD: first, the space-time development of perturbative parton cascade evolution and its interplay with the non-perturbative hadronization dynamics, and second, the issue of color correlations among the partons during the evolution, their impact on hadron formation, and their possible observable consequences for experiments. In view of the upcoming LEP2 experiments at CERN, we studied specifically e^+e^--collisions at $\sqrt{s} =$ 91 GeV and $\sqrt{s} = 170$ GeV, corresponding to the energies at LEP1 and LEP2, respectively. We emphasize however, that the issues addressed here are of general relevance to, e.g., HERA physics (both in ep and eA collisions) and Tevatron experiments ($\bar{p}p$ collisions), and experiments at RHIC (AA collisions) and the LHC (pp, pA and AA collisions).

Our analysis has been in the context of the specific approach that we have developed for describing the time evolution of a generic mixed parton/hadron system in both position and momentum space. The essential novel features of our approach are to combine kinetic theory techniques with the well-established perturbative parton evolution in momentum

space, and the use of a phenomenological model for parton-cluster recombination which is based on spatial separation as a criterion for confinement. Our kinetic description allows us to follow the time evolution of the system locally in each phase-space element $d^3r d^4k$ in a manner consistent with the uncertainty principle, and trace the evolution from the initial state all the way to the final hadron yield. Thus we "see" the time-dependence from the "hot" initial state as far as possible as the participating partons and hadrons experience it at the microscopic level. There is certainly considerable model dependence associated with our phenomenological simulation of the hadronization mechanism, but the comparisons here and in Ref. [20] with experimental data of global event properties measured at LEP1 indicate that our approach is largely consistent with the present knowledge of LEP physics.

The main findings from our numerical simulations are:

(i) The space-time development of jet evolution exhibits the characteristic features of an 'inside-outside' cascade [25, 26], in which particles are in the average produced earliest at smallest rapidity (small x), close to the spatial location of the initial vertex. Only with progressing time and increasing distances do particles populate more densely regions of higher rapidity, as we discuss in more detail below.

(ii) Color correlations are important, as seen from our comparison of three scenarios with different levels of accounting for the color degrees of freedom. These correlations occur among the partons during both the perturbative parton shower and the coalescence of partons into clusters, exhibiting themselves, e.g., in an increase of high-multiplicity events, larger average hadron multiplicities, and softer momentum spectra for the produced particles.

(iii) Our simulation of experimental jet reconstruction from the final-state hadrons and the extraction of the derived W mass spectrum raises the possibility that there may be a large upward shift in the 'observed' $m_W^{(reconstructed)}$ from the 'actual' mass $m_W^{(generated)}$, which could reach several hundred MeV. The effect of color correlations alone (40) could be as large as $\langle \Delta m_W \rangle \approx 300$ MeV, which is up to an order of magnitude larger than estimated in similar previous investigations [8, 9, 10, 11]. If true, this would have dramatic implications for the LEP2 experiments.

We must then ask why the space-time and color-correlation effects turn out to be so

large in our analysis, compared to the related investigations by, e.g., Sjöstrand and Khoze (SK) [8], and by Webber (BW) [10], who find in general that $\langle \delta m_W \rangle \approx 20 - 40$ MeV, rising possibly to ≈ 100 MeV in extreme cases. The answer is likely to be rooted in at least two essential differences between the approaches employed by SK and BW, and ours. As we have already tried to bring out, our approach incorporates an explicit causally-ordered space-time description, and a dynamical scheme of parton-hadron conversion that is formulated spatially. At this point, it is important to understand better these differences as an aid to judging the relevance of their possible implications.

The common basic concept of SK and BW is the use of well-understood angular-ordered parton shower evolution according to the leading-logarithmic QCD evolution equations in momentum space, i.e., in terms of x, and k^2 or $k_\perp^2$, in combination with a specific hadronization model, string-fragmentation in the case of SK and cluster-fragmentation in the case of BW. The perturbative parton evolution and the non-perturbative hadronization are treated independently, with an interface at some intermediate mass scale μ which plays the role of a perturbative cut-off parameter. No explicit use of space-time variables is made *a priori*, but the space-time location of each parton at the moment of hadronization can be reconstructed statistically by working backwards. This procedure does not, however, follow causally the space-time histories of all the partons including their space-time correlations, which is accomplished naturally by our forward time evolution approach. In the previous approaches, interference and cross-talk between the parton showers emanating from the W^+ and W^- decays are incorporated by allowing for the color reconnection of partons belonging to different color-singlet subsystems just before they are hadronized. At most one such color reconnection is allowed to occur in each event, i.e., out of the ensemble of final state partons only a single pair is possibly selected to be rearranged in color space. The reconnection probability which controls the strength of the effect is treated as a free parameter.

The central intuition of our approach, as applied to e^+e^- collisions, is that the intial state may be regarded as a 'hot spot' where partons are temporarily unconfined and evolve according to perturbative QCD, surrounded by a 'cold' confining medium containing non-perturbative condensates, through which hadrons propagate. During perturbative QCD shower evolution, the hot spot expands stochastically and inhomogeneously. We follow

the space-time evolution in small discrete time steps, monitoring the separations between all the partons. In this way, we keep track of all their spatial correlations during the entire shower evolution. In the particular case of $e^+e^- \rightarrow W^+W^-$, it is easy to see, as we discussed earlier, that the W^+ and W^- decay while still very close to each other and generally within a typical confinement length of about 10^{-13} cm, so that they together occupy a single 'hot spot'. We ignore the W^+ and W^- 'parentages' of the partons during the subsequent combined shower evolution. The likelihood of non-perturbative hadronization (confinement) is determined statistically by the nearest-neighbor criterion (12) alone, without regard to the parentage of the individual partons. If the W^+ and W^- showers were to overlap completely, the probabilities of 'exogamous' cluster formation by partons with different $W^\pm$ parents would be comparable with that of 'endogamous' cluster formation by partons sharing the same $W^\pm$ parent. This would lead to many more 'exogamous' clusters than the color-reconnection models proposed previously. In practice, the showers from the W^+ and W^- decays usually have different axes, and phase mismatches between high-rapidity partons in any case suppress their possible interferences, so that 'exogamy' is likely only between partons with low momenta in the center-of-mass. Nevertheless, there are many such partons, and their overlap is large, so there are many opportunities for 'exogamy', as we now discuss more quantitatively.

We recall that when W^+W^- pairs are produced at $Q = \sqrt{s} = 170$ GeV in the center-of-mass frame of the γ^*/Z^0, the $W^\pm$ are to first approximation created at rest, because their boost factors are $\gamma^\pm \simeq Q/(2m_W) = 1.05 \approx 1$. As pointed out in 3.1.1, the difference Δt between the times at which the W^+ and W^- decay is short on a typical hadronic scale: $\Delta t = |t^+ - t^-| \simeq 0.1\ fm$. Suppose, for definiteness, that the W^+ decays first. Then, for a time span Δt the produced $q_1\bar{q}_2$ system evolves undisturbed, just as in ordinary 2-jet events. A parton shower develops, spreading rapidly out in configuration space, analogously to the illustration in Fig. 6. In space-time, the $q_1\bar{q}_2$ pair and the increasing number of accompanying bremsstrahlung partons expand like in a shock wave [20] from the decay vertex. Most of the activity is concentrated in cones around the leading q_1 and $\bar{q}_2$. The situation is illustrated in Fig. 16, where we define the initial 2-jet orientation as the z^+-axis. Although the particles commonly move outward close to the speed of light with velocities determined by their invariant mass k^2, the the region of space-time extent that

they occupy depends sensitively on the energy fractions x via the uncertainty principle. As a consequence, the leading partons ($x = O(1)$) become separated from the wee partons ($x \lesssim 10^{-2}$). This is an important effect of time dilation and Lorentz contraction [25, 26]. In fact, the q_1 and $\bar{q}_2$ moving along the z^+-axis form the forefront of the expanding shell, which has a proper thickness $\Delta z^{proper} \simeq 1/m_W$, implying

$$\Delta z_q \;=\; \Delta z_{\bar{q}} \;\equiv\; \frac{\Delta z^{proper}}{2\,\gamma^+} \;\simeq\; \frac{1}{2\,\gamma^+\,E^+} \;\approx\; 10^{-3}\;fm\;, \tag{43}$$

whereas the wee partons, in particular the softest ones which are emitted earliest by the q_1 and $\bar{q}_2$, are smeared out by the uncertainty principle over a comparably large longitudinal extent,

$$\Delta z_{wee} \;\equiv\; \frac{1}{2\,(k_z)_{wee}} \;\simeq\; \frac{1}{2\,x\;E^+} \;\approx\; 0.1 - 1\;fm \qquad (\text{for } x \approx 10^{-2} - 10^{-3})\;. \tag{44}$$

This spatial uncertainty associated with the particles' momenta implies that the low-momentum quanta are not all concentrated at the shock front, as one would naively expect for massless particles, but rather occupy the whole interior of the expanding volume, with the wee partons piling up around the center, as depicted graphically in Fig. 16.

In this environment the W^- now decays about 0.1 fm after the showering of the $q_1\bar{q}_2$ system from the W^+ has already produced a significant number (of the order of 10) wee partons around its vertex at $\vec{r}^{\,+}$, producing a second $q_3\bar{q}_4$ pair which expands around $\vec{r}^{\,-}$ in the same fashion. The second jet system is produced within the wee-parton cloud of the first one, which had been created *in vacuo*. Therefore, as suggested by Fig. 17, these later partons experience a 'medium' of surrounding wee partons, immediately opening up the possibility of interactions due to correlations. The leading $q_3\bar{q}_4$ (plus possibly a few large-x partons) of the second jet system are well separated in rapidity $y \simeq \ln x$ from the small-x wee partons, and therefore decouple and escape essentially unscathed [6]. On the other hand, the wee partons produced in W^+ decay and those emitted by the later W^- decay can interact easily, because they are in the same range of y (x) and moreover overlap in their spread of spatial directions (44).

These expectations are borne out by Fig. 18, which illustrates the fractions of clusters that are formed 'endogamously', i.e., by partons from the same W decay shower, and 'exogamously', i.e., by interactions between partons from different W showers. The clusters formed by endogamous unions of partons from the $W^\pm$ are labelled by $\mathcal{E} = 0, 1$, respectively,

and clusters formed by exogamous union between partons from the W^+ and the W^- are labelled by $\mathcal{E} = 1/2$. In some cases, the partons emitted during cluster formation combine to form other clusters with $\mathcal{E} = 1/4, 3/4$, etc.. We see in Fig. 18 that there are in general several exogamous unions per event, and that these are more common among the less-energetic clusters, as suggested qualitatively in the previous paragraph. (For comparison, in the hypothetical case of inifinitely separated W^+ and W^- decay vertices, where 'exogamy' is excluded, the distributions would be peaked at 0 and 1, and vanishing in between.) We notice also that our our preferred *Color-Full* scenario III produces the largest fraction of exogamous clusters, as one would expect qualitatively, in view of the larger number of allowed diagrams shown in Fig. 5. In our interpretation, it is the large number of these exogamous unions that is primarily responsible for the large mass shift in eq. (40).

We believe that these intuitive arguments provide a plausible origin for the large non-perturbative correlation effects found in our approach. We would like to emphasize that the space-time picture outlined above is, in its general features, independent of the particular Lorentz frame employed, as has been discussed especially by Bjorken [25] and by Kogut and Susskind [26]. A Lorentz boost between different frames can distort the picture, but the characteristic 'inside-outside' evolution in both rapidity and longitudinal direction is always the same. We think that any such 'inside-outside' space-time picture will lead to considerable overlap, correlation and interaction among the wee partons from the W^+ and the W^- (c.f. Fig 17). These effects are subject to the general constraints of relativity and the uncertainty principle, but one must make explicit use of space-time variables if one wishes to model them realistically. In our approach the causal evolution is followed in a probabilistic manner, with the phase-space density of particles at any point of time being determined by the preceding history, and in turn governing the statistical occurrence of parton-cluster coalescence, according to the local particle density and the nearest-neighbor criterion (12). On the other hand, a pure momentum-space description cannot take correlation effects fully into account, which may lead to a substantial underestimate of the possible effects on observable quantities such as the W mass.

Some final comments are appropriate here. It has to be stressed that the systematic shift δm_W that we find in the W mass is dependent on our specific modelling of the non-perturbative parton-cluster formation, as can be seen from the fact that it depends on

the color scenarios (I)-(III) which are used. We recall that we have not considered color rearrangement on the perturbative level, and that its effects have been estimated to be very small, $\delta m_W^{pert.} \lesssim 5$ MeV [8], and not comparable with our results (37), $\delta m_W \simeq 300 - 400$ MeV. As we have emphasized repeatedly, the non-perturbative aspects have been modelled rather differently in SK and BW, and we cannot prove that our results are more reliable. However, we believe that our results demonstrate that the effects of color flow dynamics during the non-perturbative parton-hadron conversion are model-dependent, and that one must be cautious in drawing conclusions from an incomplete set of different approaches. It will be possible to test models for W^+W^- hadronization using measurements of final-state hadron distributions in both longitudinal and transverse momenta for different relative orientations of the $W^\pm$ decay jets. This may enable the development of strategies for the measurement of m_W that are insensitive to complexities associated with low-momentum hadrons that have been the central theme of this paper. It remains to be seen what the experiments at LEP2 will soon reveal.

We close by emphasizing that the effects discussed here become of increasing importance as one considers more complex systems with larger particle densities: perhaps already in deep-inelastic lepton-hadron scattering or hadronic collisions at very small x, but certainly in reactions involving nuclei, such as eA or pA, where partons propagate through and interact with nuclear matter, and especially in AA where multiple (mini)jets (up to many hundreds for large A) evolve simultanously and interact.

ACKNOWLEDGEMENTS

We thank Valery Khoze and Yuri Dokshitzer for encouraging discussions, and appreciate useful suggestions by Leif Lönnblad. Also we thank Brookhaven National Laboratory for generously providing computer time on its RHIC-cluster.

References

[1] Yu. L. Dokshitzer, V. A. Khoze, A. H. Mueller, and S. I. Troyan, Rev. Mod. Phys. **60**, 373 (1988); and, *Basics of Perturbative QCD*, Advanced Series on Directions in High Energy Physics, Vol. 5 (Editions Frontieres, Gif-sur-Yvette Cedex, France, 1991).

[2] Ya. I. Azimov, Yu. L. Dokshitzer, V. A. Khoze and S. I. Troyan, Z. Phys. **C27**, 65 (1985); Yu. L. Dokshitzer, V. A. Khoze and S. I. Troyan, Z. Phys. **C55**, 107 (1992).

[3] T. Hebbeker, Phys. Rep. **217**, 69 (1992); S. Bethke and J. E. Pilcher, Ann. Rev. Nucl. Part. Sci. **42**, 251 (1992); M. Schmelling, Phys. Scripta **51**, 683 (1995).

[4] V. A. Khoze, L. H. Orr, and W. J. Stirling, Nucl. Phys. **B378**, 413 (1992).

[5] Yu. L. Dokshitzer, V. A. Khoze, L. H. Orr, and W. J. Stirling, Nucl. Phys. **B403**, 65 (1993).

[6] V. S. Fadin, V. A. Khoze, and A. D. Martin, Phys. Lett. **B320**, 141 (1994); Phys. Rev. **D49**, 2247 (1994).

[7] G. Gustafson, U. Pettersson, and P. Zerwas, Phys. Lett. **B209**, 90 (1988).

[8] T. Sjöstrand and V. A. Khoze, Phys. Rev. Lett. **72**, 28 (1994); Z. Phys. **C62**, 281 (1994).

[9] G. Gustafson and J. Häkkinen, Z. Phys. **C64**, 659 (1994).

[10] B. Webber, Talk given at the *LEP2 QCD work group meeting*, May 1995; and in *QCD Event Generators*, ed. I. G. Knowles and T. Sjöstrand, *Proceedings of the Workshop "Physics at LEP2"*, CERN Yellow Report. (1995) (in preparation).

[11] L. Lönnblad, CERN-TH. 95-218 (1995).

[12] S. Todorova, in *QCD Event Generators*, ed. I. G. Knowles and T. Sjöstrand, *Proceedings of the Workshop "Physics at LEP2"*, CERN Yellow Report. (1995) (in preparation).

[13] A. Gaidot, J. P. Pansart, and N. K. Watson, OPAL TN320 (1995).

[14] B. Andersson, G. Gustafson, G. Ingelman and T. Sjöstrand, Phys. Rep. **97**, 33 (1983).

[15] G. Marchesini and B. R. Webber, Nucl. Phys. **310**, 461 (1988).

[16] K. Geiger, Phys. Rep. **258**, 237 (1995).

[17] K. Geiger, CERN-TH. 95-181 (1995) (hep-ph/9507365).

[18] K. Konishi, A. Ukawa, and G. Veneziano, Nucl. Phys. **B157**, 45 (1979).

[19] A. Bassetto, M. Ciafaloni and G. Marchesini, Nucl. phys. **B163**, 477 (1980); Phys. Rep. **100**, 203 (1983).

[20] J. Ellis and K. Geiger, Phys. Rev. **D52**, 1500 (1995); Nucl. Phys. **A590**, 609 (1995).

[21] A detailed comparitive study of Monte Carlo generators for hadronic e^+e^--events can be found in: K. Hamacher and M. Weierstall, DELPHI 95-80 PHYS 515 (1995).

[22] T. Sjöstrand, Comp. Phys. Com. **82**, 74 (1994).

[23] G. Marchesini, B. R. Webber, G. Abbiendi, I. G. Knowles, M. H. Seymour and L. Stanco, Comp. Phys. Com. **67**, 465 (1992).

[24] L. Lönnblad, Comp. Phys. Com. **71**, 15 (1992).

[25] J. D. Bjorken, *Proceedings of the 1973 Summer Institute of Particle Physics*, SLAC-167 (1973); and in *Current Induced Reactions*, Lecture Notes in Physics, Vol. 56, (Springer, New York 1976).

[26] J. Kogut and L. Susskind, Phys. Rep. **8**, 75 (1973); A. Casher, J. Kogut and L. Susskind, Phys. Rev. Lett. **31**, 792 (1973).

[27] B. A. Campbell, J. Ellis, and K. A. Olive, Phys. Lett. **B235**, 325 (1990); Nucl. Phys. **B345**, 57 (1990).

[28] J. Ellis, Nucl. Phys. **B2**, 478 (1970).

[29] K. Geiger, Phys. Rev. **D46**, 4986 (1992), *ibid.* **D47**, 133 (1993).

[30] D. Amati and G. Veneziano, Phys. Lett. **B83**, 87 (1979); D. Amati, A. Bassetto, M. Ciafaloni, G. Marchesini, and G. Veneziano, Nucl. Phys. **B173**, 429 (1980).

[31] L. Caneschi and A. Schwimmer, Phys. Lett. **B86**, 179 (1979); H. Minekata, Phys. Rev. Lett. **45**, 325 (1980).

[32] K. Konishi, CERN-TH. 2853 (1980); G. Marchesini, L. Trentadue and G. Veneziano, Nucl. Phys. **B181**, 335 (1981).

[33] K. Geiger and B. Müller, Phys. Rev. **D50**, 337 (1994); K. Geiger, Phys. Rev. **D50**, 3243 (1994).

[34] B. R. Webber, in *Proceedings of the XXVII-th International Conference on High Energy Physics (ICHEP)*, Glasgow 1994.

[35] Yu. L. Dokshitzer, Sov. Phys. JETP **46**, 641 (1977); G. Altarelli and G. Parisi, Nucl. Phys. **B126**, 298 (1977).

[36] Yu. L. Dokshitzer, D. I. Dyakonov, and S. I. Troyan, Phys. Rep. **58**, 269 (1980).

[37] B. R. Webber, Nucl. Phys. **B238**, 492 (1984).

[38] R. Hagedorn, *Thermodynamics of Strong Interactions*, Cargèse Lectures in Physics, Vol. 6 (1973).

[39] See e.g.: Particle Data Group, *Review of Particle Properties*, Phys. Rev. **D50**, 1173 (1994).

[40] E. P. Wigner, Phys. Rev. **98**, 145 (1955); M. L. Goldberger and K. M. Watson, *Collision Theory* (Wiley, New York, 1964).

[41] JADE Collaboration, W. Bartel *et al.*, Z. Phys. **C33**, 23 (1986).

[42] S. Catani, Yu. L. Dokshitzer, M. Olsson, G. Turnock, and B. R. Webber, Phys. Lett. **B269**, 432 (1991).

[43] L. Lönnblad and T. Sjöstrand, Phys. Lett. **B351**, 293 (1995).

TABLE CAPTIONS

Table 1:

Average multiplicities of produced partons and hadrons from simulations of $e^+e^- \to Z^0 \to hadrons$ at $Q = \sqrt{s} = 91$ GeV. For each of the color scenarios (I)-(III), the experimental number for the total charged multiplicity was used to fix the minimum parton virtuality μ_0 during the perturbative shower activity. With this constraint, all other numbers emerge as predictions.

Table 2:

Results for the color scenarios (I)-(III) of average multiplicity, size and mass of clusters formed from coalescing partons in $e^+e^- \to Z^0 \to hadrons$ at 91 GeV, as well as the relative contributions of the different cluster formation subprocesses of Fig. 5.

Table 3:

Listing of average properties of $e^+e^- \to \gamma^*/Z^0 \to W^+W^- \to hadrons$ at $Q = \sqrt{s} =$ 170 GeV resulting from the simulations for the color scenarios (I)-(III). The same values for the minimum parton virtuality μ_0 as in Table 1 were used. Mean multiplicities of partons, hadrons, and charged particles are shown, as well as the averages of charged particle transverse momentum $p_\perp^{ch}$ (with respect to the thrust axis), energy fraction $x_E^{ch} = 2E^{ch}/Q$, and thrust T.

Table 4:

Average cluster properties in $e^+e^- \to \gamma^*/Z^0 \to W^+W^- \to hadrons$ at 170 GeV for each of the color scenarios (I)-(III). In correspondence to Table 2, the average multiplicity, size and mass of clusters are listed, and the associated relative contributions of the different cluster formation subprocesses of Fig. 5.

Table 5:

Compilation of the mass shifts resulting from the various investigations discussed in the text. As before, (I), (II) and (III) refer to the 'color-blind', 'color-singlet', and 'color-full' scenario, respectively. The subscripts 'real' and 'hypo' label the two discussed extremes of the *realistic* situation (expected close-by decays of the W^+ and W^-), and a *hypothetical*

case (with infinitely-separated W^+ and W^- decay vertices). The top part refers to the jet-selection scheme (33), and we compare the reconstructed average mass $\langle m_W^{(rec.)} \rangle = \langle m^+ + m^- \rangle / 2$, the mass shifts $\langle \Delta m_W \rangle = \langle m_W^{(gen.)} \rangle - \langle m_W^{(rec.)} \rangle$, where the mean generated W mass is $\langle m_W^{(gen.)} \rangle = 79.75$ GeV, and the widths $\sigma(\delta m_W)$ of the associated distributions (Fig. 15). The lower part of the table presents the corresponding quantities extracted by using the jet-selection scheme (41).

FIGURE CAPTIONS

Figure 1:

Illustration of the dynamical connection between the three basic process types described by the equations (8)-(10): a cascade develops first as a shower with parton multiplication, followed by coalescence of partons to color-singlet clusters, and finally the decay of clusters into hadrons.

Figure 2: Schematics of the *nearest-neighbor criterion*, eq. (12). Two partons may coalesce to a cluster if they are nearest neighbors in space-time, and if their mutual separation L_{12} approaches the confinement scale L_c, with a probability given by the width of the transition interval $[L_0, L_c]$ (c.f. eq. (14)), which originates from the form of the confinement potential V in (5).

Figure 3:

Example of color-singlet combinations of partons in a quark jet which form independent subsystems, and of color-connected partons which screen the color of the original quark.

Figure 4:

Diagrammatic rules for the color flow structure in parton branching processes, connecting quarks and gluons coming in and going out of a vertex. Each quark (antiquark) is accompanied in its direction of motion by a color (anticolor) line, and each gluon carries both a color and an anticolor line.

Figure 5:

Diagrammatic rules for the color flow structure in the various cluster formation processes. Each quark (antiquark) carries a color (anticolor) line, and each gluon carries both a color and an anticolor line. Note that the restriction to color-singlet configurations of two coalescing partons is equivalent to considering only the three diagrams in the left column. The remaining four diagrams require additional parton emission to ensure local color conservation.

Figure 6:

Illustration of the space-time development of the parton shower, cluster formation by parton coalescence, and cluster decay into hadrons in an $e^+e^- \to Z^0 \to q\bar{q}$ event. The time intervals for the propagation of intermediate particles are determined by the particles' 4-momenta and the uncertainty principle.

Figure 7:

Time development and conversion from parton to hadron degrees of freedom in $e^+e^- \to$ *hadrons* at $Q = \sqrt{s} = 91$ GeV in the center-of-mass frame. We show the time dependences of the total number of 'live' partons (hadrons), their respective total energies $E = \sum_i E_i$, total longitudinal momentum fraction $x = 2/Q \sum_i k_{z\,i}$, and their summed transverse momentum $k_\perp = \sum_i \sqrt{k_{x\,i}^2 + k_{y\,i}^2}$, where the z-axis is defined along the jet direction. The three curves correspond to the three color scenarios (I)-(III) defined in the text.

Figure 8:

Effects of the three color scenarios (I)-(III) on cluster size distribution and cluster mass spectrum (top), and on the rapidity and transverse momentum distribution of produced hadrons (bottom), in $e^+e^- \to$ *hadrons* at 91 GeV.

Figure 9:

Time development of momentum and spatial distribution of partons present in the system at given times. The top parts show rapidity and transverse-momentum spectra, whereas the bottom plots show longitudinal and transverse spatial distributions, where the z-axis is defined along the jet direction. The various curves correpond to different time steps during the evolution as specified in the top left corner. To guide the eye, the arrows indicate the direction of time change.

Figure 10: Time development of hadron distributions in correspondence to the parton spectra of Fig. 9. The different curves show the contributions at the time steps given in the top left corner.

Figure 11:

Two-dimensional plots of the ratios of hadrons to the sum over partons plus hadrons, eq. (25). The top part shows the spectrum in rapidity versus $\log(t)$, where t is the time in

the center-of-mass frame. The bottom part shows the corresponding distribution along the jet (z-) axis. The 'inside-outside' evolution in both y and z with increasing time is clearly seen.

Figure 12:

General situation of initial 4-jet production in $e^+e^- \to \gamma^*/Z^0 \to W^+W^- \to hadrons$. The W^+ and W^- are simultanously produced at t_0 by the γ^*/Z^0, and then decay into jet pairs $q_1\bar{q}_2$ and $q_3\bar{q}_4$, at delayed times t^+ and t^- with $|t^+ - t^-| \lesssim 0.1\ fm$.

Figure 13:

Results from the *realistic* (full curves) and the *hypothetical* (dotted curves) evolution of the W^+W^- system defined in the text. We show the cluster mass spectrum, transverse momentum of produced hadrons, and multiplicity distribution of charged particles.

Figure 14:

Results for the color scenarios (I)-(III) from the simulated reconstruction of the W^+W^- 4-jet system according to the jet-finding algorithm explained in the text. The top part shows the mass spectrum of the reconstructed four jets (before imposing cuts on m_{jet}), whereas the bottom part shows the fraction of the total three-momentum of particles carried by the four reconstructed jets: $X := \sum_i^4 |\vec{p}_i^{\,jet}| / \sum_j^n |\vec{p}_j^{\,par}|$.

Figure 15:

Results of the simulation of experimental W mass reconstruction for the three color scenarios (I)-(III). The top part shows the distribution of the reconstructed m_W and, as reference, the generated W mass distribution from the Breit-Wigner spectrum. The bottom part shows the resulting mass shift distribution $\Delta m_W = m_W^{(generated)} - m_W^{(reconstructed)}$. with mean values given by (36).

Figure 16:

Graphical illustration of the space-time geography of jet evolution (part 1): on the left, the situation of the $q_1\bar{q}_2$ jet system produced in empty space by the first decaying W (here the W^+). In accordance with the 'inside-outside' cascade picture, the small-x wee partons are emitted the earliest and occupy the largest longitudinal spatial region due to the uncertainty associated with their momentum. They form the bulk of radiated particles.

The leading quark (antiquark) and the most energetic large-x partons, on the other hand, are localized around the expanding shock front of the system. The right part shows the same situation in the familiar longitudinal $t-z$ plane, where the leading particles separate along the light cone, and the wee partons fill the central region. Here t^+ refers to the time in the $q_1\bar{q}_2$ rest-frame, and z^+ to the jet axis.

Figure 17:

Graphical illustration of the space-time geography of jet evolution (part 2): the left side shows the situation now for both jet pairs, $q_1\bar{q}_2$ from the W^+ and $q_3\bar{q}_4$ from the W^-. Due to the large spatial smearing of the small-x wee partons, there is a significant region of overlap in which interactions among the partons from the two jet systems can cause correlations. The right side illustrates as in a) the situation in the $t-z$ plane, where t^+ (t^-) and z^+ (z^-) correspond to the time and the jet-axis of the $q_1\bar{q}_2$ ($q_3\bar{q}_4$) jet pair system. Because at $\sqrt{s} = 170$ GeV the Lorentz factors $\gamma^{\pm} \simeq 1$, one has $t^+ \simeq t^-$ so that $t \equiv (t^+ + t^-)/2$ approximately measures the common time. Note also that due to the relative azimuthal angle of the 2 jet systems, the z^+ and z^- axes are generally rotated, so that the indicated region of wee parton overlap is generally asymmetric.

Figure 18:

Normalized distributions of the 'endogamous/exogamous' parentage of clusters formed in W^+W^- events at $\sqrt{s} = 170$ GeV. The shower-initiating $q_1\bar{q}_2$ ($q_3\bar{q}_4$) pairs from the W^+ (W^-) decay carry $\mathcal{E} = 0$ ($\mathcal{E} = 1$). In branching processes, each endogamous daughter parton i carries the previous generation's value, i.e. $\mathcal{E}_i = \mathcal{E}_{i-1}$, and each cluster formed by exogamous coalescence of partons i and j carries $\mathcal{E}_c = (\mathcal{E}_i + \mathcal{E}_j)/2$. The figure compares the $\mathcal{E}$-distributions corresponding to the color scenarios (I)-(III). The top (middle) (bottom) part shows all ('fast': $x > 0.01$)('slow': $x < 0.01$) clusters, respectively.

$e^+e^- \to Z^0 \to$ *hadrons*, $E_{cm} = 91$ GeV

Multiplicities:

Quantity	I	II	III	Experiment [3, 21]
$\langle n^{ch} \rangle$		21.0 (input)		20.95 ± 0.88
μ_0 (GeV)	0.8	1.1	1.5	–
$\langle n_{par} \rangle$	24.9	24.2	19.1	–
$\langle n_{had} \rangle$	41.3	42.5	43.2	–
$\langle n_{par} \rangle / \langle n_{had} \rangle$	0.60	0.57	0.44	–
$\langle n^{\pi^\pm} \rangle$	16.6	15.8	17.7	17.1 ± 0.4
$\langle n^{\pi^0} \rangle$	10.2	11.4	10.8	9.9 ± 0.08
$\langle n^{K^\pm} \rangle$	2.79	3.06	2.39	2.42± 0.13
$\langle n^{K^0} \rangle$	2.46	2.97	2.03	2.12± 0.06
$\langle n^{\rho^\pm} \rangle$	2.88	3.09	2.93	–
$\langle n^{\rho^0} \rangle$	1.48	1.90	1.67	1.40± 0.1
$\langle n^{p} \rangle$	0.72	0.55	0.80	0.92± 0.11
$\langle n^{\Lambda^0} \rangle$	0.33	0.27	0.39	0.348 ± 0.013

Table 1

$e^+e^- \rightarrow Z^0 \rightarrow$ *hadrons*, $E_{cm} = 91$ GeV

Cluster properties:

Quantity	I	II	III
$\langle n_{clu} \rangle$	22.6	21.5	23.2
$\langle n_{par} \rangle / \langle n_{clu} \rangle$	1.10	1.13	0.82
$\langle n_{clu} \rangle / \langle n_{had} \rangle$	0.55	0.51	0.53
$\langle R_{clu} \rangle$ (fm)	0.92	0.89	0.97
$\langle M_{clu} \rangle$ (GeV)	1.71	1.86	1.67
$g + g \rightarrow C + C$	52.3 %	37.2 %	8.4 %
$g + g \rightarrow C + g$	–	–	15.7 %
$g + g \rightarrow C + g + g$	–	–	33.0 %
$q + \bar{q} \rightarrow C + C$	11.3 %	9.9 %	2.8 %
$q + \bar{q} \rightarrow C + g$	–	–	3.1 %
$q + g \rightarrow C + q$	36.4 %	52.9 %	13.0 %
$q + g \rightarrow C + q + g$	–	–	23.8 %

Table 2

$e^+e^- \to W^+W^- \to$ *hadrons*, $E_{cm} = 170$ GeV

Multiplicities and global event properties:

Quantity	I	II	III
μ_0 (GeV)	0.8	1.1	1.5
$\langle n_{par} \rangle$	37.4	36.8	29.6
$\langle n_{had} \rangle$	68.5	70.7	72.2
$\langle n_{par} \rangle / \langle n_{had} \rangle$	0.55	0.52	0.41
$\langle n^{ch} \rangle$	36.1	37.3	37.5
$\langle n^{ch} \rangle_{\lvert y \rvert <1}$	29.3	30.3	30.8
$\langle\, p_\perp^{ch} \,\rangle$ (GeV)	1.90	1.83	1.75
$\langle\, x_E^{ch} \,\rangle$ ($\times 10^{-2}$)	2.85	2.74	2.59
$\langle\, 1-T \,\rangle$ ($\times 10^{-2}$)	6.0	7.1	6.5

Table 3

$e^+e^- \to W^+W^- \to$ *hadrons*, $E_{cm} = 170$ GeV

Cluster properties:

Quantity	I	II	III
$\langle n_{clu} \rangle$	37.0	34.8	38.9
$\langle n_{par} \rangle / \langle n_{clu} \rangle$	1.01	1.06	0.76
$\langle n_{clu} \rangle / \langle n_{had} \rangle$	0.54	0.50	0.53
$\langle R_{clu} \rangle$ (fm)	0.92	0.89	0.97
$\langle M_{clu} \rangle$ (GeV)	1.76	1.97	1.62
$g + g \to C + C$	47.5 %	32.6 %	5.9 %
$g + g \to C + g$	–	–	15.3 %
$g + g \to C + g + g$	–	–	25.8 %
$q + \bar{q} \to C + C$	12.8 %	11.2 %	2.0 %
$q + \bar{q} \to C + g$	–	–	4.4 %
$q + g \to C + q$	39.7 %	56.2 %	14.5 %
$q + g \to C + q + g$	–	–	32.2 %

Table 4

$e^+e^- \to W^+W^- \to$ *hadrons*, $E_{cm} = 170$ GeV

Compilation of mass shifts from m_W reconstruction:

Quantity (in GeV)	I	II	III
1st reconstruction scheme, eq. (33)			
$\langle m_W^{(rec.)} \rangle_{real}$	80.13	80.53	80.45
$\langle \Delta m_W \rangle_{real}$	0.383	0.812	0.706
$\sigma(\Delta m_W)_{real}$	2.65	3.05	3.02
$\langle m_W^{(rec.)} \rangle_{hypo}$	80.15	80.55	80.18
$\langle \Delta m_W \rangle_{hypo}$	0.396	0.806	0.424
$\sigma(\Delta m_W)_{hypo}$	2.90	3.28	3.25
2nd reconstruction scheme, eq. (41)			
$\langle m_W^{(rec.)} \rangle_{real}$	80.13	80.30	80.21
$\langle \Delta m_W \rangle_{real}$	0.413	0.899	0.788
$\sigma(\Delta m_W)_{real}$	2.64	2.92	2.96
$\langle m_W^{(rec.)} \rangle_{hypo}$	80.13	80.28	80.01
$\langle \Delta m_W \rangle_{hypo}$	0.422	0.889	0.512
$\sigma(\Delta m_W)_{hypo}$	2.80	3.06	3.08

Table 5

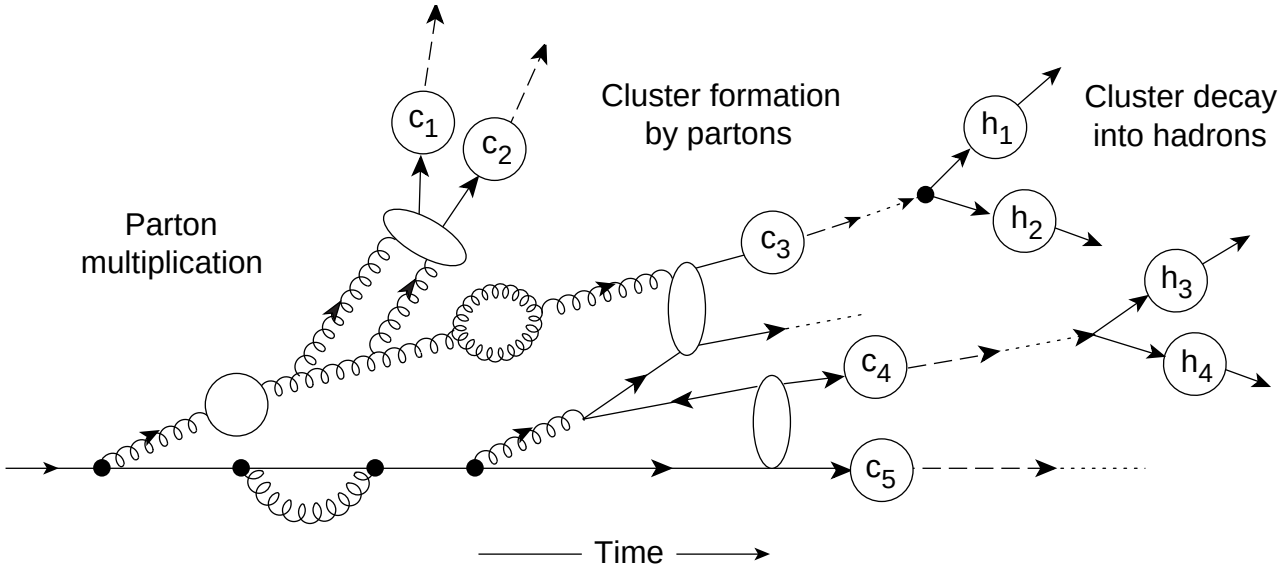
Parton
multiplication
Cluster formation
by partons
Cluster decay
into hadrons
c1
c2
c3
c4
c5
h1
h2
h3
h4
Time

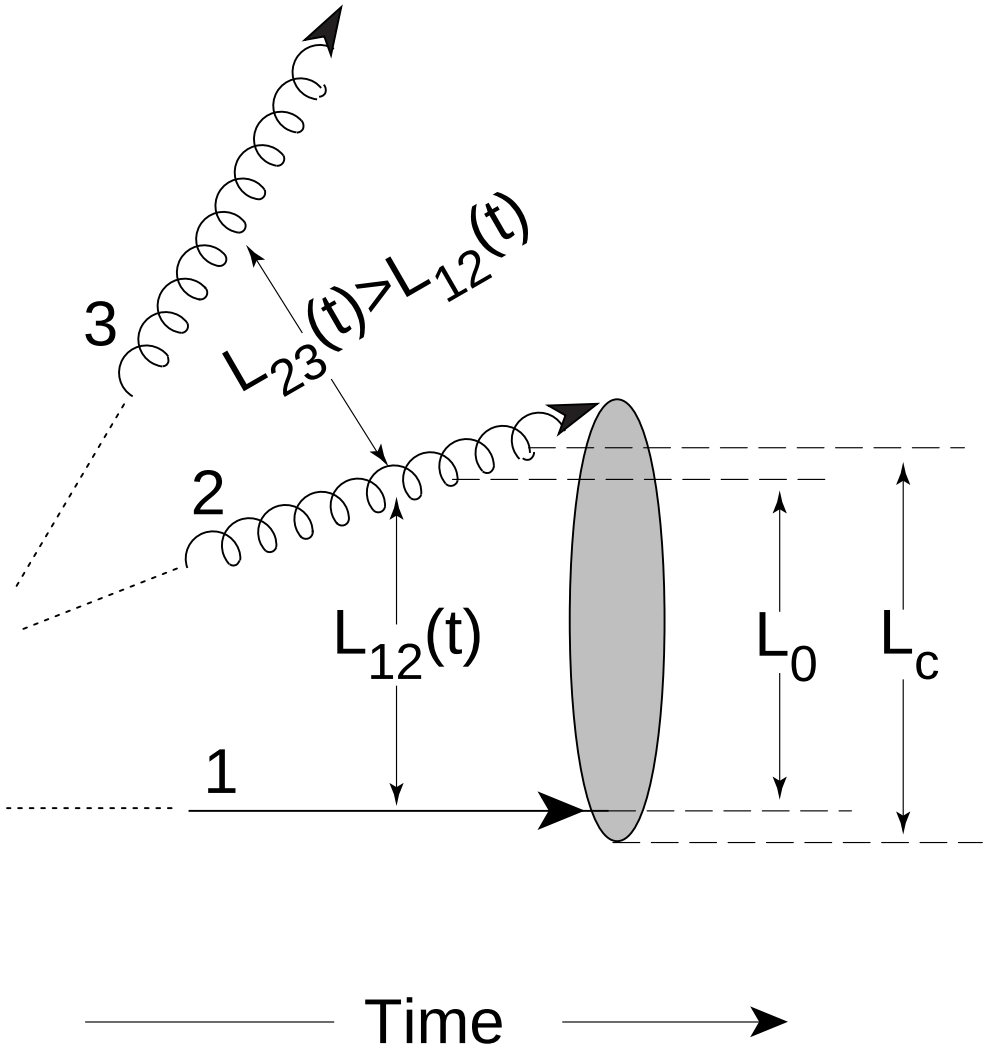
3
$L_{23}(t) > L_{12}(t)$
2
$L_{12}(t)$
L_0
L_c
1
Time

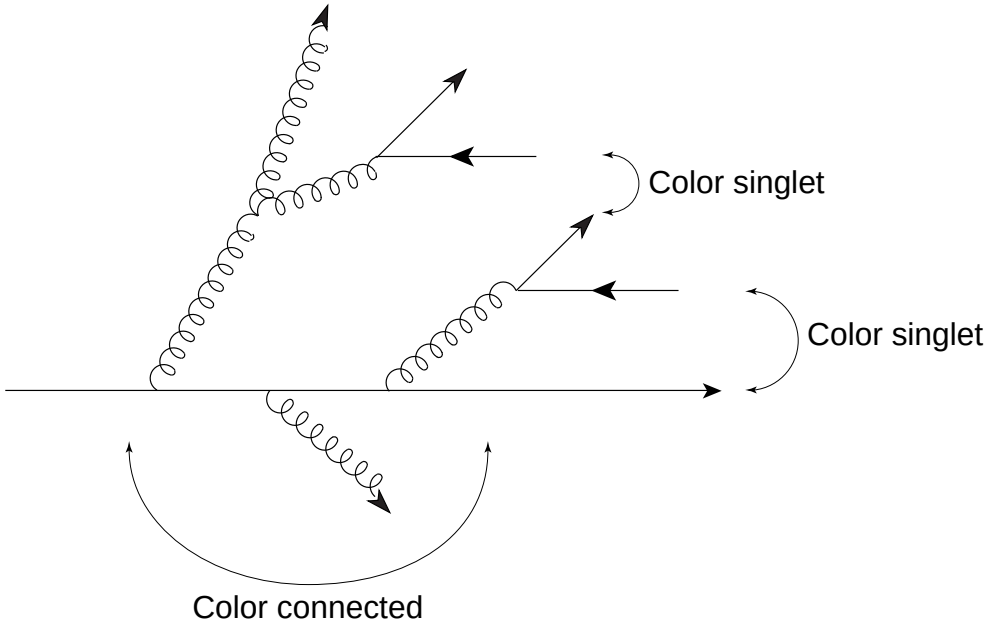
Color singlet
Color singlet
Color connected

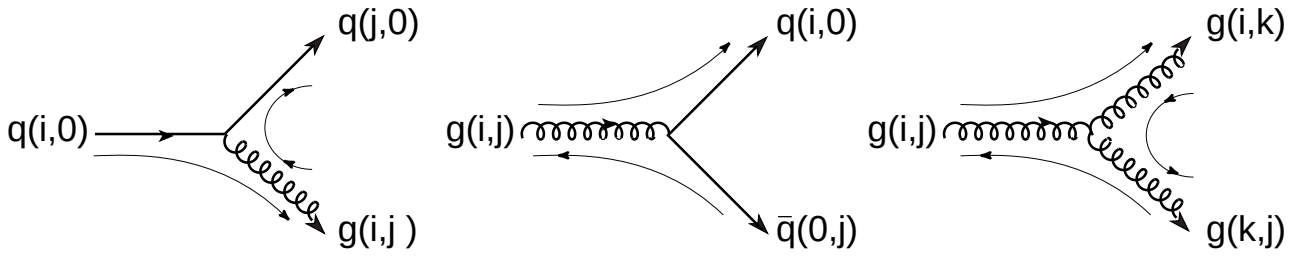
q(i,0)
q(j,0)
g(i,j)
g(i,j)
q(i,0)
q̄(0,j)
g(i,j)
g(i,k)
g(k,j)

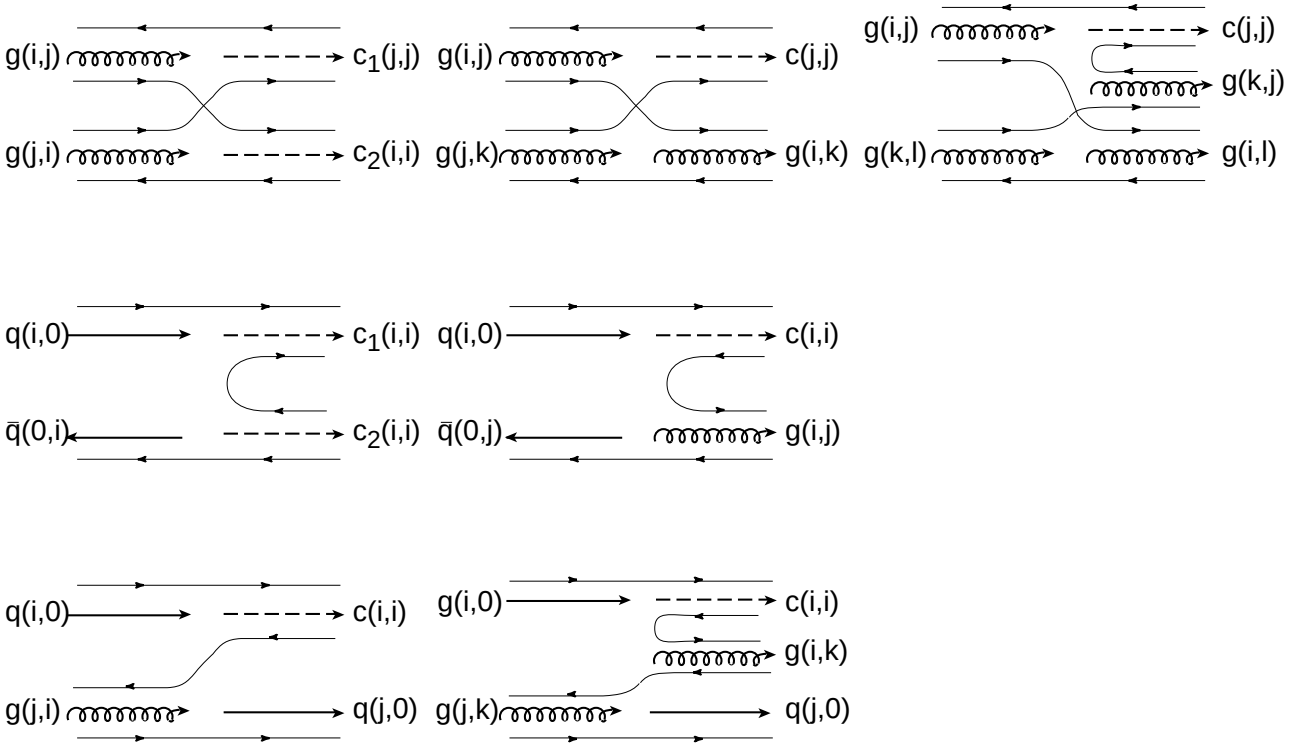
g(i,j)
c1(j,j)
g(j,i)
c2(i,i)
g(i,j)
c(j,j)
g(j,k)
g(i,k)
g(i,j)
c(j,j)
g(k,j)
g(k,l)
g(i,l)
q(i,0)
c1(i,i)
q̄(0,i)
c2(i,i)
q(i,0)
c(i,i)
q̄(0,j)
g(i,j)
q(i,0)
c(i,i)
g(j,i)
q(j,0)
g(i,0)
c(i,i)
g(i,k)
g(j,k)
q(j,0)

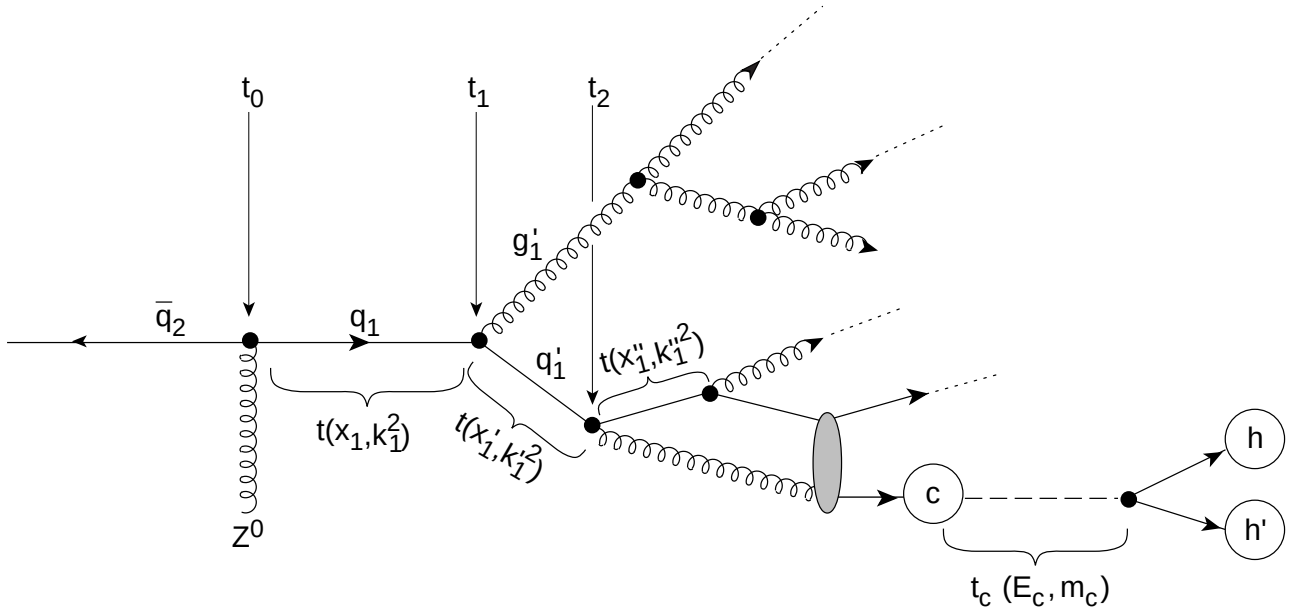
t0
t1
t2
g'1
q̄2
q1
q'1
t(x''1,k''1 2)
t(x1,k1 2)
t'(x'1,k'1 2)
Z0
c
h
h'
tc (Ec, mc)

TIME EVOLUTION OF PARTICLES AND 4-MOMENTUM

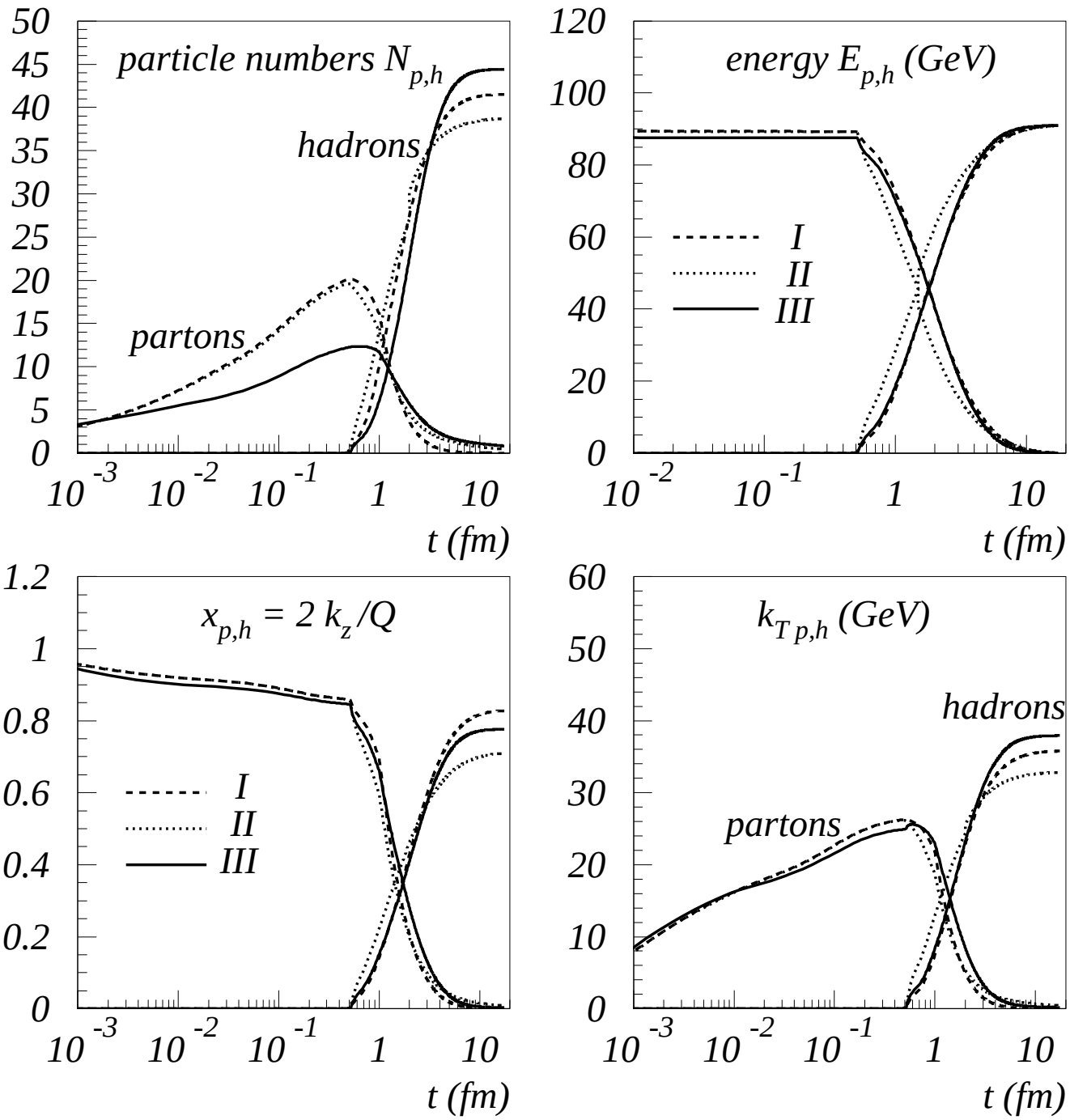

CLUSTER AND HADRON SPECTRA

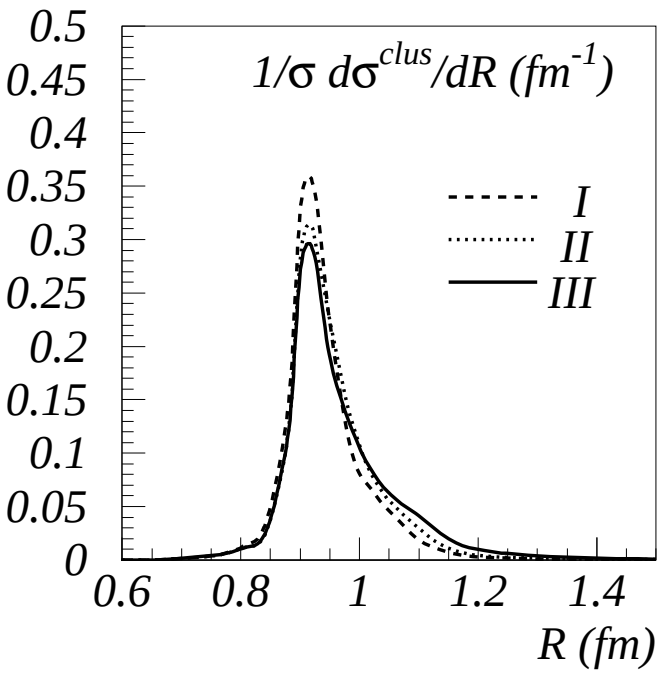

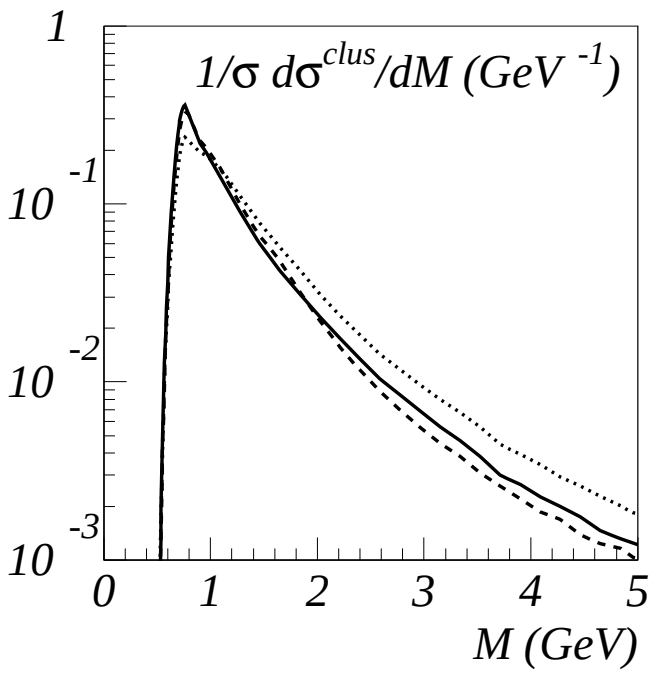

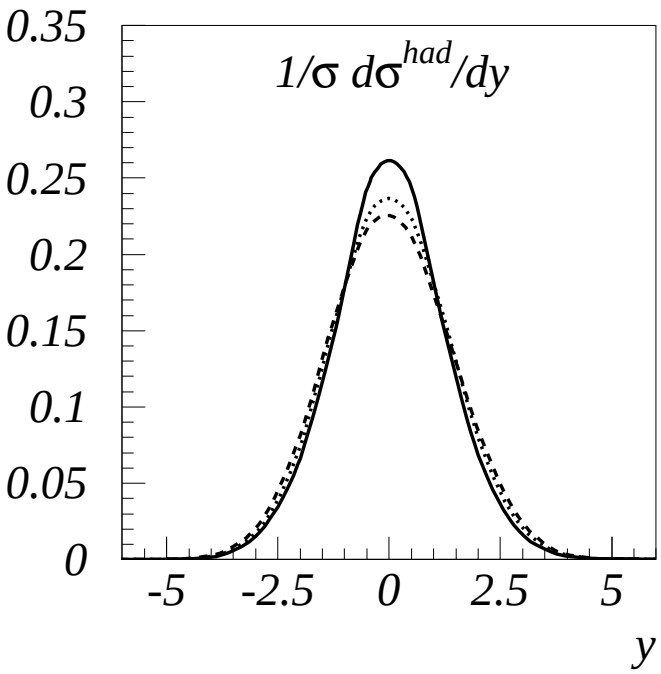

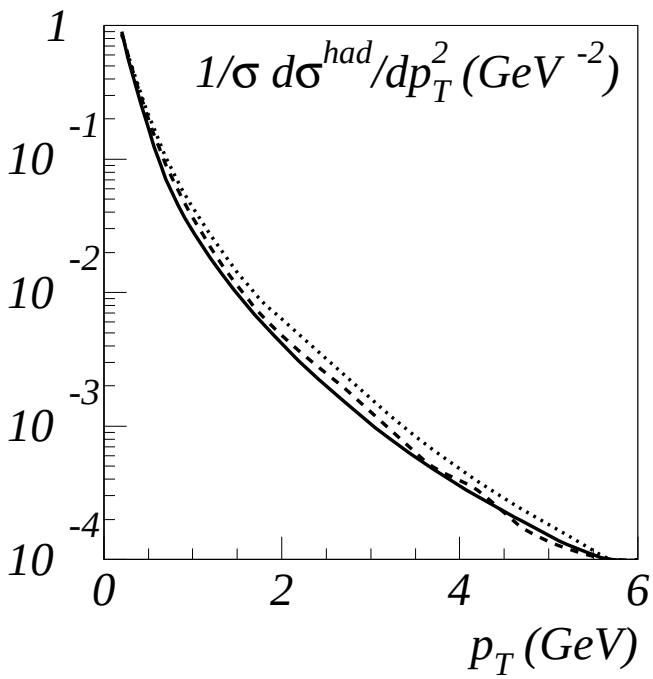

TIME EVOLUTION OF PARTON SPECTRA

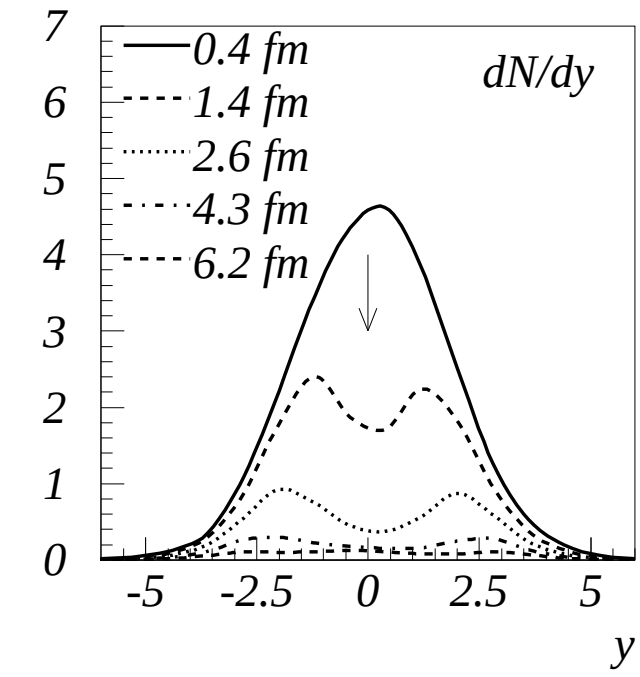

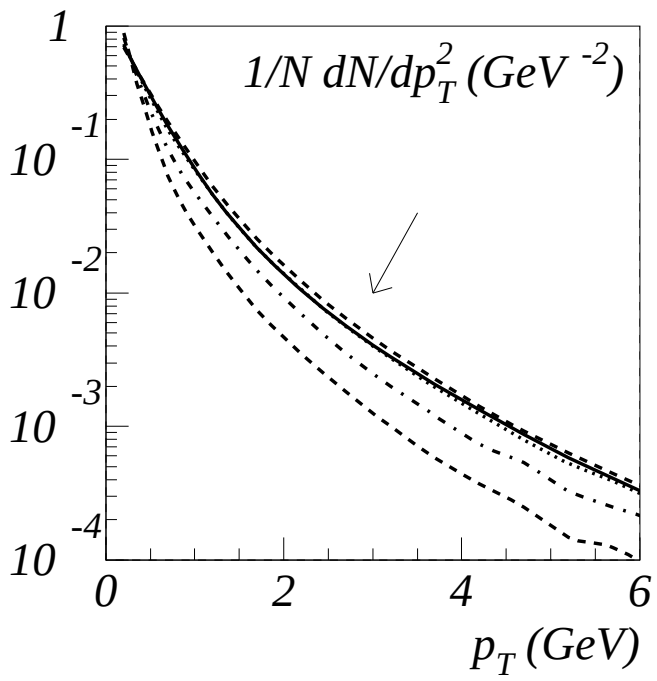

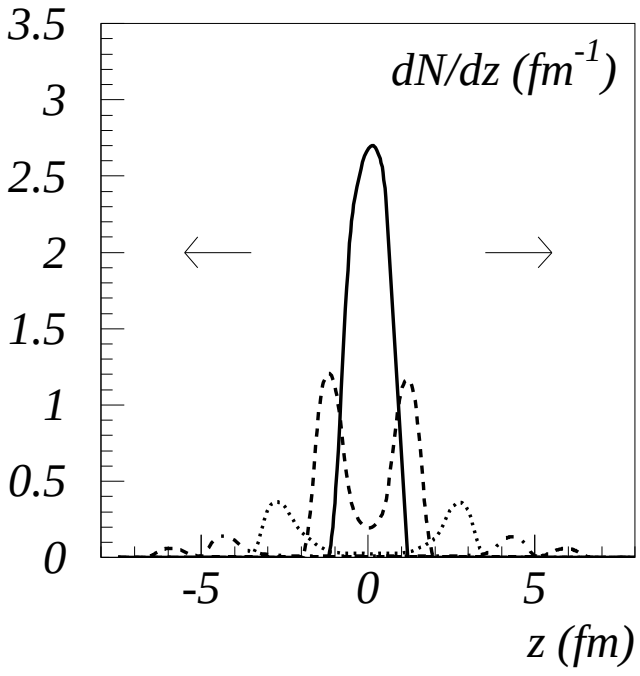

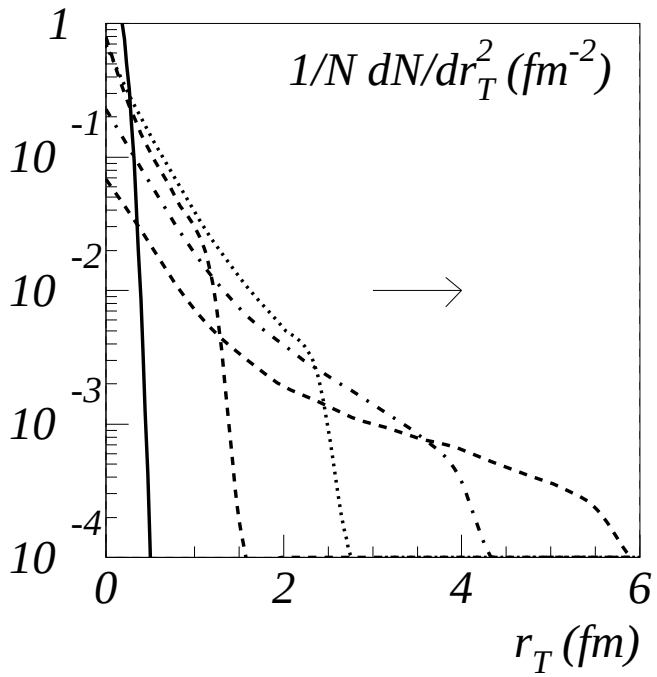

TIME EVOLUTION OF HADRON SPECTRA

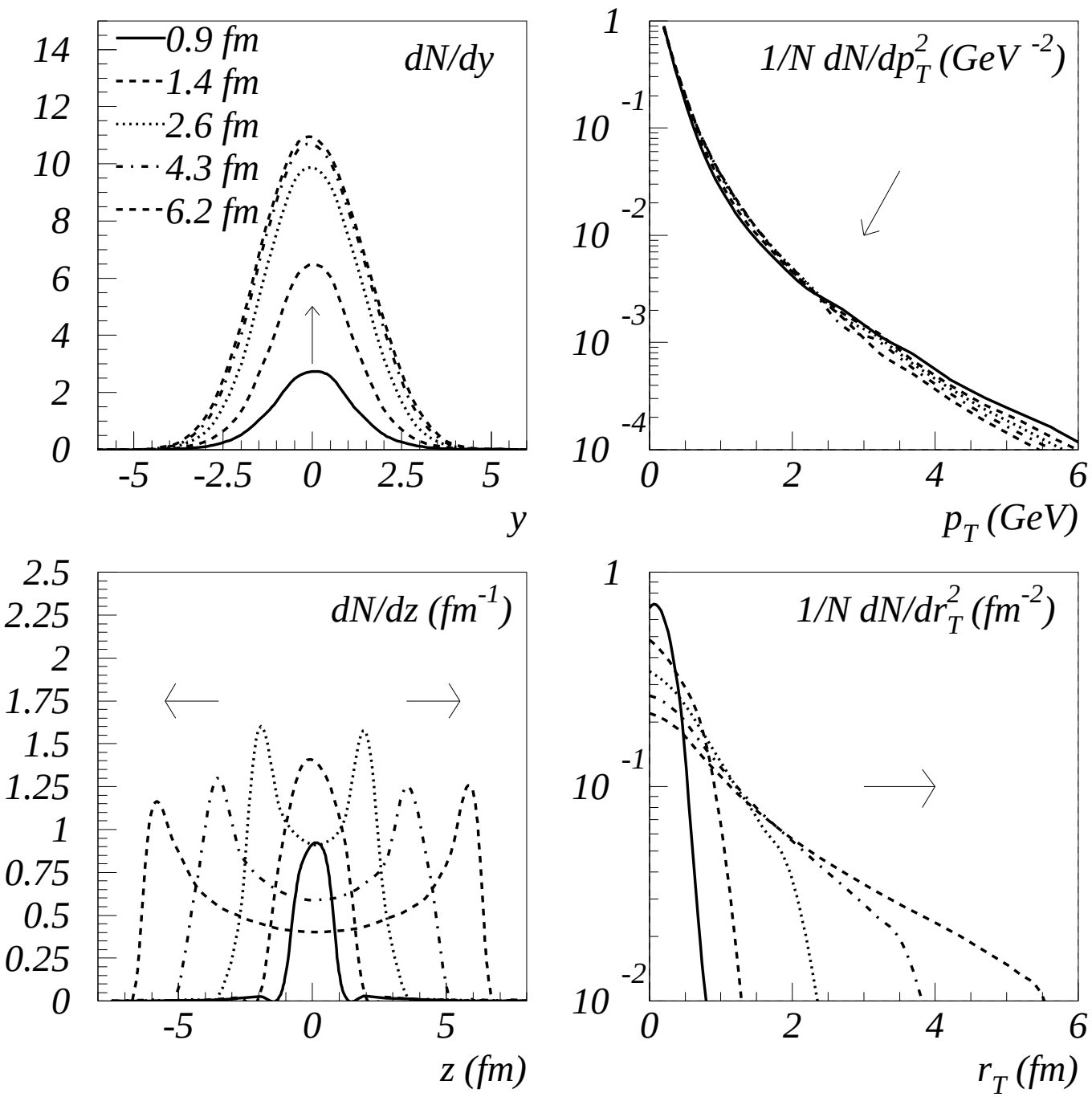

INSIDE-OUTSIDE HADRON FORMATION

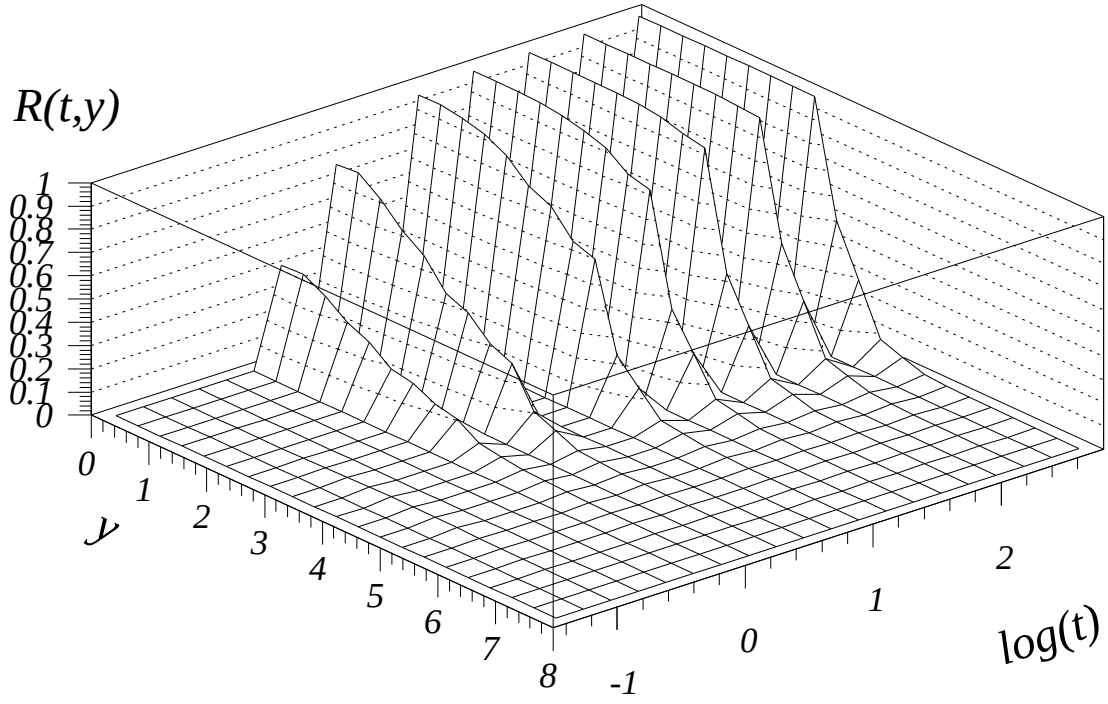

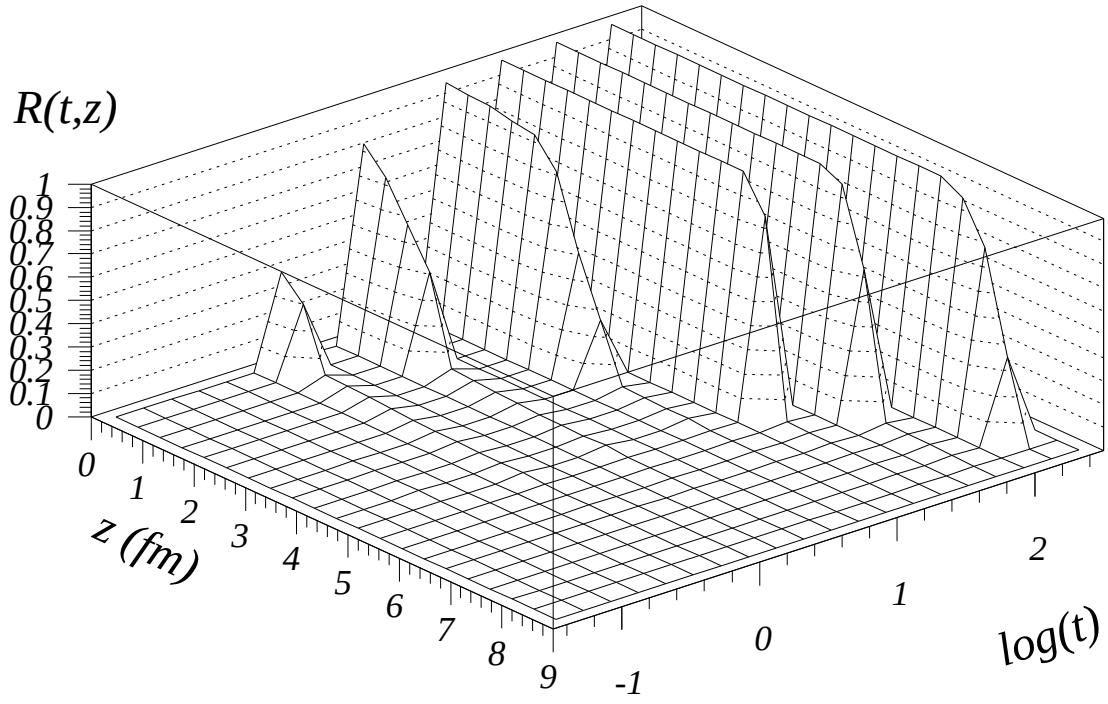

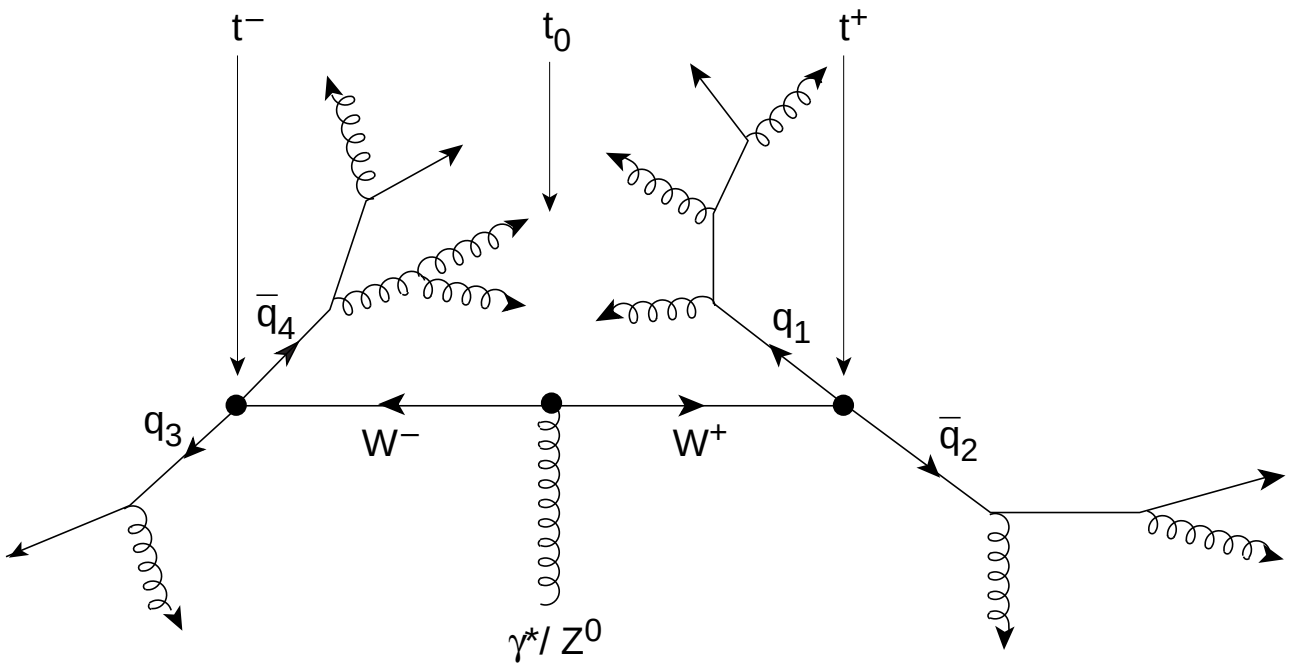
t−
t0
t+
q̄4
q1
q3
W−
W+
q̄2
γ*/ Z0

REAL VS. HYPOTHETICAL W^+W^- DECAY

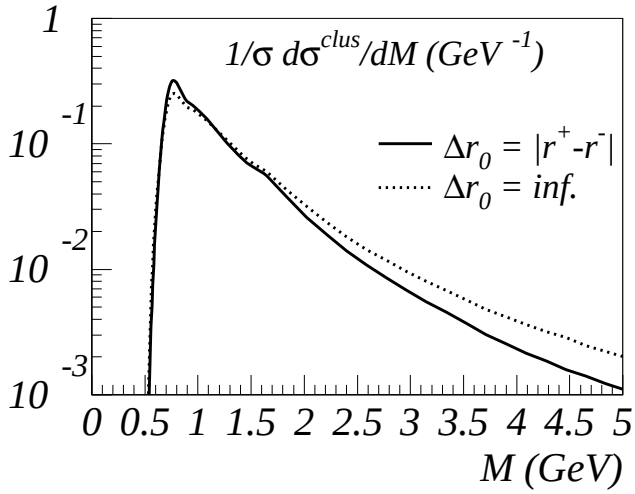

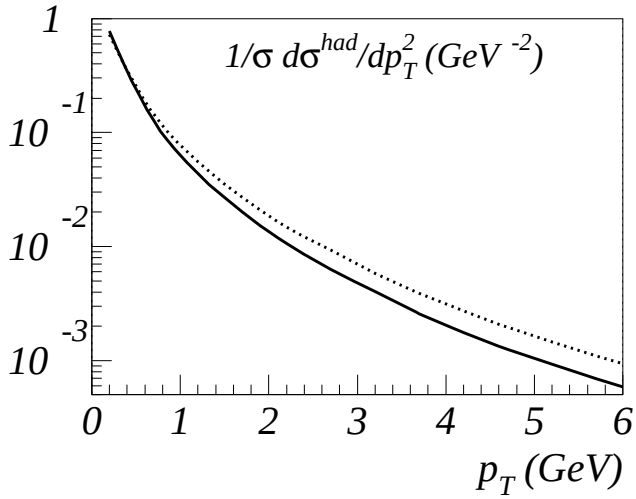

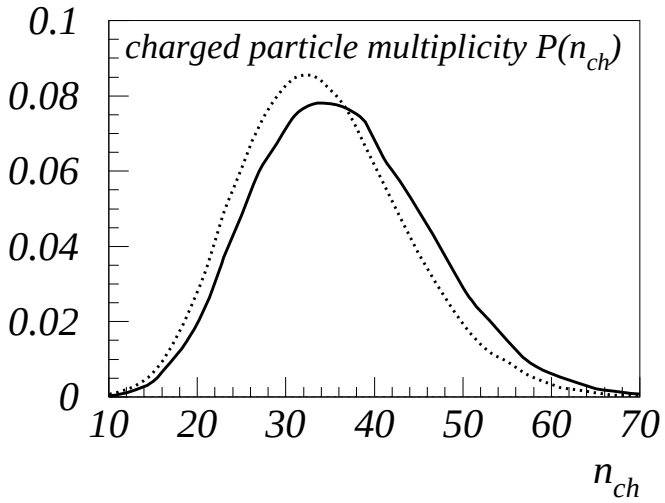

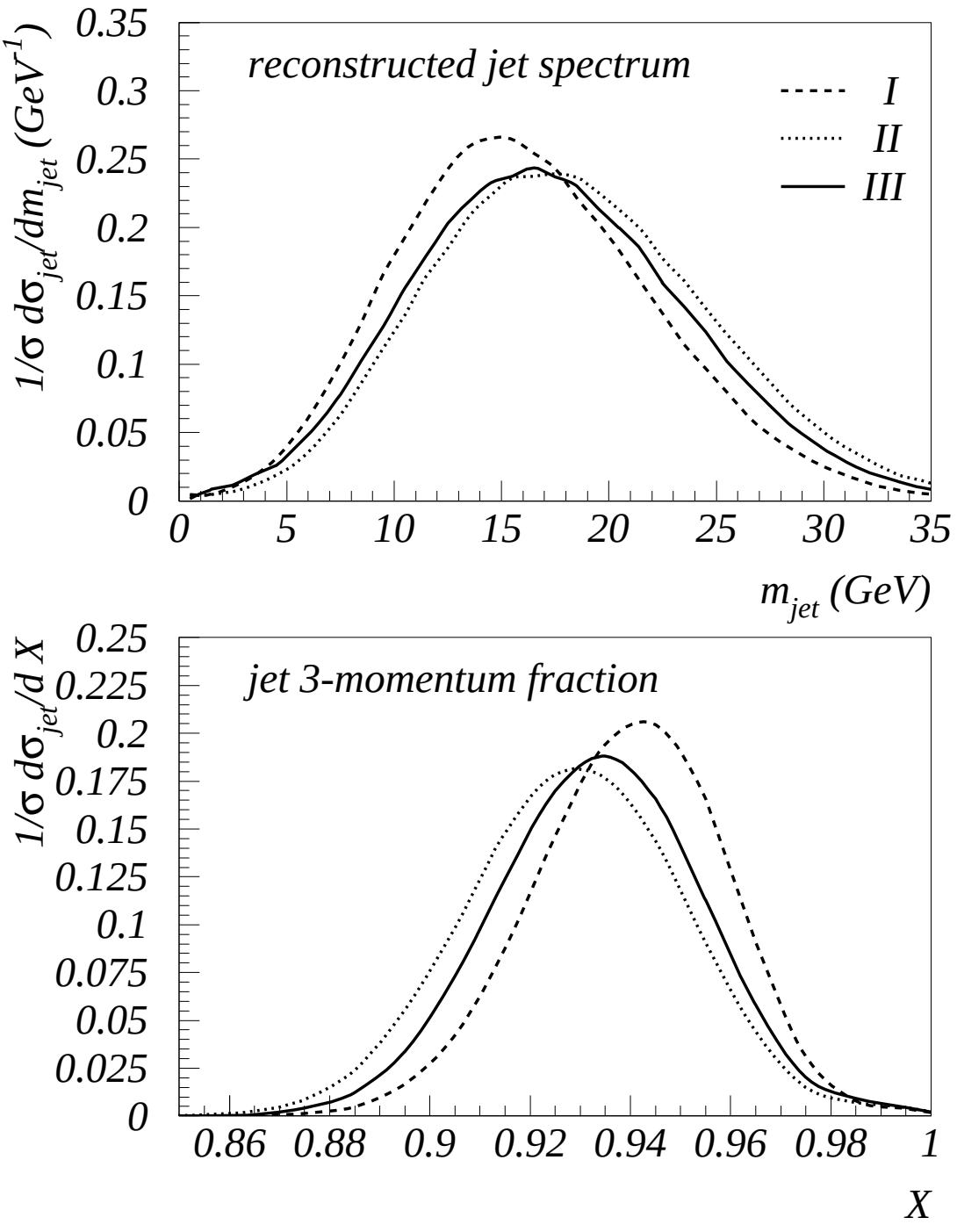
reconstructed jet spectrum
I
II
III
1/σ dσ_jet/dm_jet (GeV^-1)
0.35
0.3
0.25
0.2
0.15
0.1
0.05
0
0
5
10
15
20
25
30
35
m_jet (GeV)
jet 3-momentum fraction
1/σ dσ_jet/d X
0.25
0.225
0.2
0.175
0.15
0.125
0.1
0.075
0.05
0.025
0
0.86
0.88
0.9
0.92
0.94
0.96
0.98
1
X

W-MASS ANALYSIS

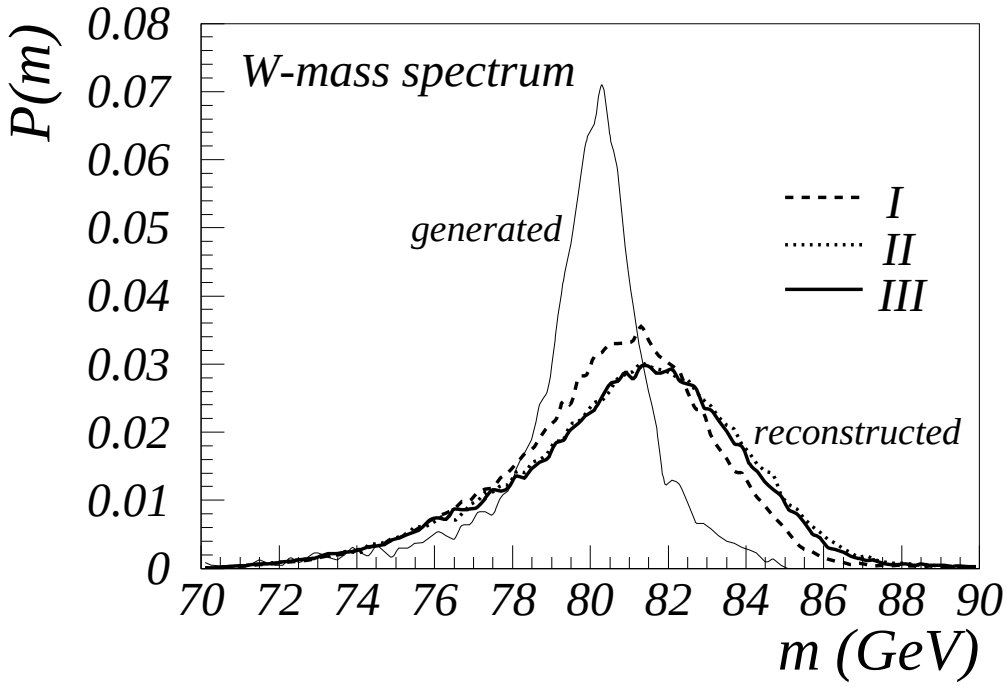

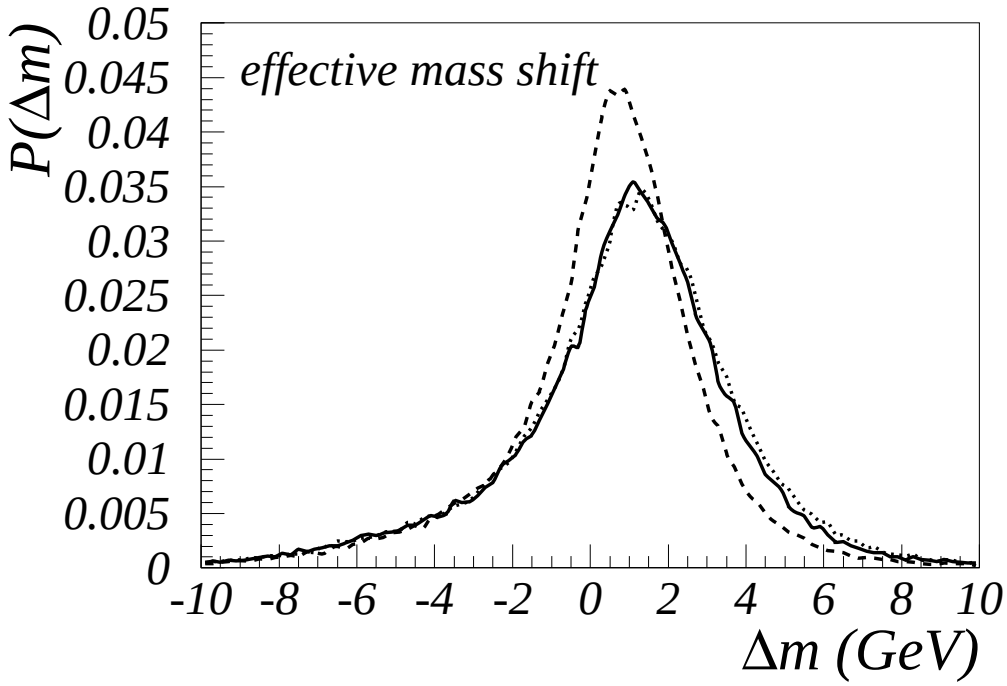

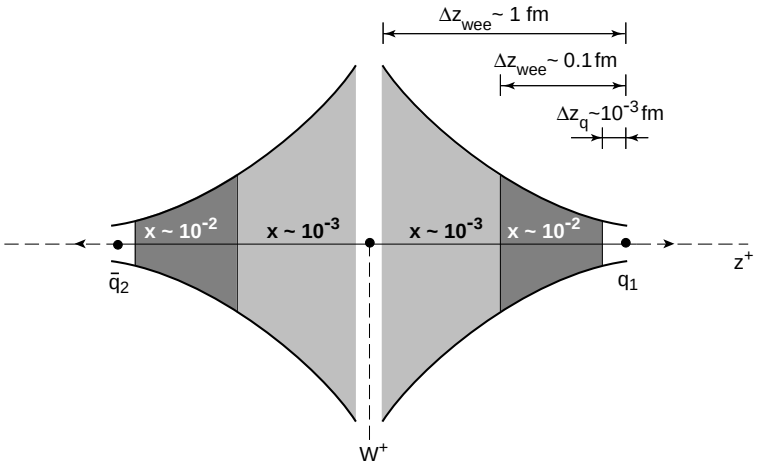
Δz_wee ~ 1 fm
Δz_wee ~ 0.1 fm
Δz_q ~ 10^-3 fm
x ~ 10^-2
x ~ 10^-3
x ~ 10^-3
x ~ 10^-2
q̄2
q1
z+
W+

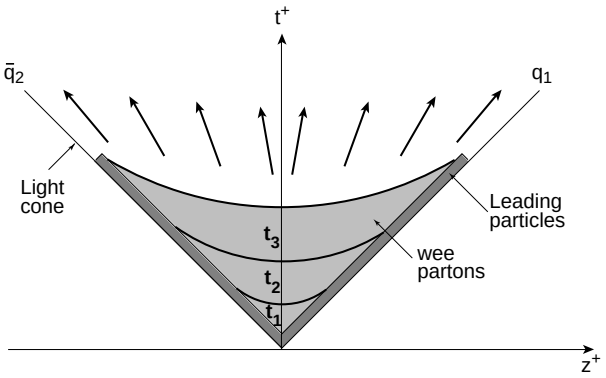
t+
q̄2
q1
Light cone
Leading particles
wee partons
t3
t2
t1
z+

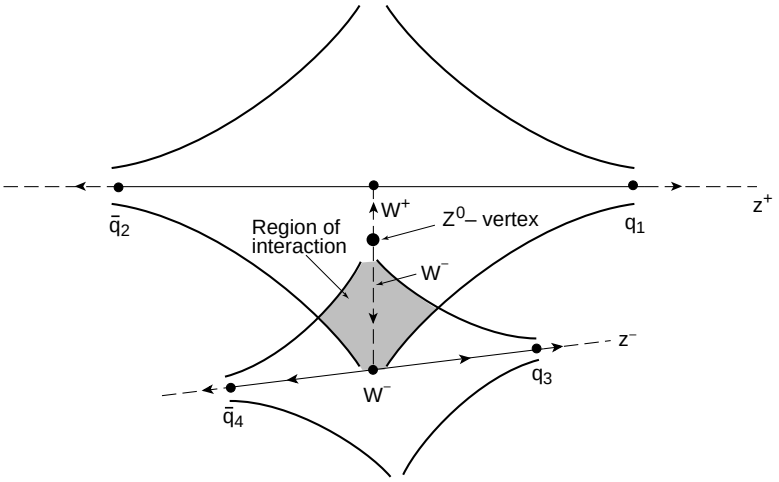
$\bar{q}_2$
Region of interaction
W^+
Z^0– vertex
q_1
z^+
W^-
z^-
q_3
W^-
$\bar{q}_4$

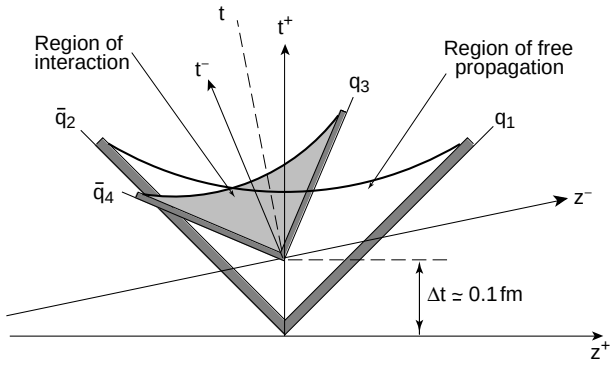
t
t^+
Region of interaction
t^-
q_3
Region of free propagation
$\bar{q}_2$
q_1
$\bar{q}_4$
z^-
$\Delta t \simeq 0.1\,\mathrm{fm}$
z^+

DEGREE OF EXOGAMY